NASA TECHNICAL REPORT

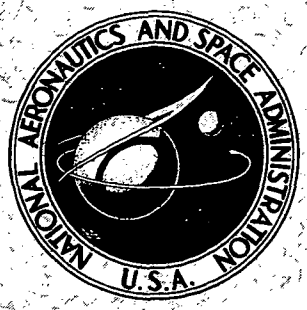

NASA TR R-397

NASA TR R-397

AN ANALYSIS OF THE RELAXATION OF LAMINAR BOUNDARY LAYER ON A FLAT PLATE AFTER PASSAGE OF AN INTERFACE WITH APPLICATION TO EXPANSION-TUBE FLOWS

by Roop N. Gupta

Langley Research Center
Hampton, Va. 23365

NATIONAL AERONAUTICS AND SPACE ADMINISTRATION • WASHINGTON, D. C. • DECEMBER 1972

1. Report No.	2. Government Accession No.	3. Recipient's Catalog No.
NASA TR R-397		

4. Title and Subtitle	5. Report Date
AN ANALYSIS OF THE RELAXATION OF LAMINAR BOUNDARY LAYER ON A FLAT PLATE AFTER PASSAGE OF AN INTERFACE WITH APPLICATION TO EXPANSION-TUBE FLOWS	December 1972
	6. Performing Organization Code
7. Author(s)	8. Performing Organization Report No.
Roop N. Gupta [1]	L-8514
	10. Work Unit No.
9. Performing Organization Name and Address	502-07-01-02
NASA Langley Research Center Hampton, Va. 23365	11. Contract or Grant No.
	13. Type of Report and Period Covered
12. Sponsoring Agency Name and Address	Technical Report
National Aeronautics and Space Administration Washington, D.C. 20546	14. Sponsoring Agency Code

15. Supplementary Notes

[1] NRC-NASA Resident Research Associate.

16. Abstract

The relaxation of the accelerating-gas boundary layer to the test-gas boundary layer over a flat plate in an expansion tube is analyzed. Several combinations of test gas and acceleration gas are considered. The problem is treated in two conically similar limits: (1) when the time lag between the arrival of the shock and the interface at the leading edge of the plate is very large, and (2) when this lag is negligible. The time-dependent laminar-boundary-layer equations of a binary mixture of perfect gases are taken as the flow-governing equations. This coupled set of differential equations, written in terms of the Lam-Crocco variables, has been solved by a line-relaxation finite-difference technique. The results presented include the Stanton number and the local skin-friction coefficient as functions of shock Mach number and the nondimensional distance-time variable. The results indicate that more than 95 percent of the test-gas boundary layer exists over a length, measured from the leading edge of the plate, equal to about three-tenths of the distance traversed by the interface in the free stream.

17. Key Words (Suggested by Author(s))	18. Distribution Statement
Unsteady boundary layers Binary diffusion Numerical analysis Expansion-tube flow	Unclassified – Unlimited

19. Security Classif. (of this report)	20. Security Classif. (of this page)	21. No. of Pages	22. Price*
Unclassified	Unclassified	77	$3.00

*For sale by the National Technical Information Service, Springfield, Virginia 22151

CONTENTS

AN ANALYSIS OF THE RELAXATION OF LAMINAR BOUNDARY LAYER ON A FLAT PLATE AFTER PASSAGE OF AN INTERFACE WITH APPLICATION TO EXPANSION-TUBE FLOWS

By Roop N. Gupta*
Langley Research Center

SUMMARY

The relaxation of the accelerating-gas boundary layer to the test-gas boundary layer over a flat plate in an expansion tube is analyzed. Several combinations of test gas and acceleration gas are considered. The problem is treated in two conically similar limits: (1) when the time lag between the arrival of the shock and the interface at the leading edge of the plate is very large, and (2) when this lag is negligible. The time-dependent laminar-boundary-layer equations of a binary mixture of perfect gases are taken as the flow-governing equations. This coupled set of differential equations, written in terms of the Lam-Crocco variables, has been solved by a line-relaxation finite-difference technique. The results presented include the Stanton number and the local skin-friction coefficient as functions of shock Mach number and the nondimensional distance-time variable. The results indicate that more than 95 percent of the test-gas boundary layer exists over a length, measured from the leading edge of the plate, equal to about three-tenths of the distance traversed by the interface in the free stream.

INTRODUCTION

An expansion tube (ref. 1), a facility for producing high-enthalpy gas flows, is one of the aerodynamic testing devices in which the test-flow duration is very brief. Consequently, the successful use of such a device makes it necessary to understand the nature of the flow development over the test model and the time required to attain steady flow conditions, and, in turn, requires a detailed knowledge of the time-dependent viscous-flow processes. In the case of an expansion tube, the model is first immersed in the flow of the accelerating gas prior to the arrival of the test gas and, thus, it is necessary to know the time required for the accelerating-gas boundary layer to relax to the test-gas boundary layer. The inviscid flow relaxes more rapidly than the boundary layer. For the case of a flat plate, the inviscid flow may be assumed to be fully developed in the

---

*NRC-NASA Resident Research Associate.

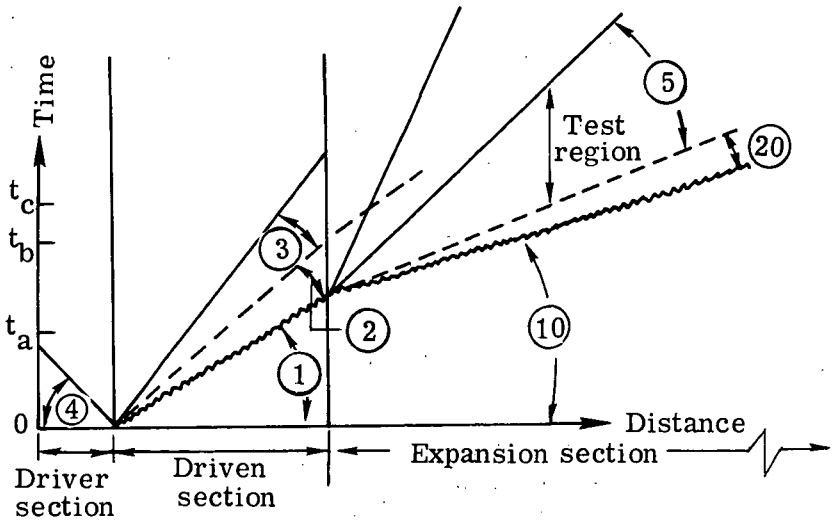

(a) Distance-time plot.

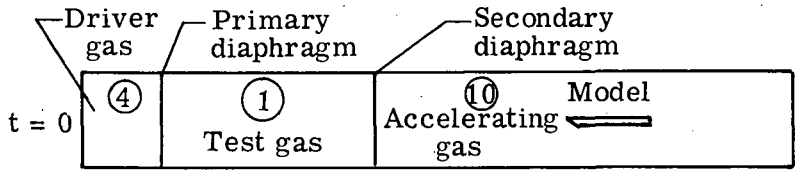

(b) Prior to run, $t = 0$.

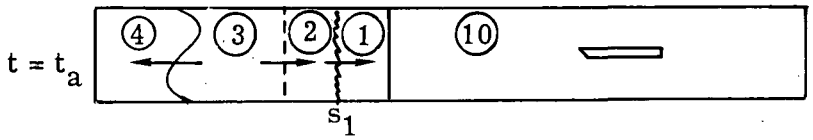

(c) After primary diaphragm burst, $t = t_a$.

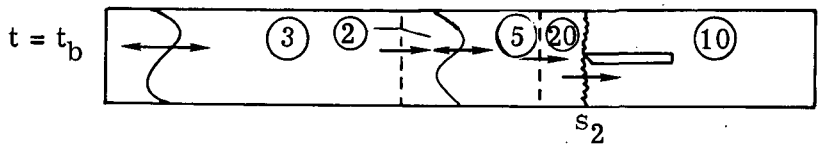

(d) After secondary diaphragm burst, $t = t_b$.

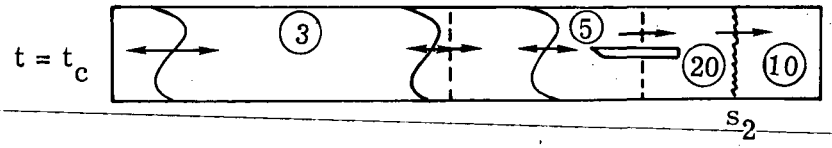

(e) During testing, $t = t_c$.

Figure 1.- Schematic diagram of an expansion-tube operation cycle. (Taken from ref. 1, circled numbers are explained therein.)

time taken by the particle in the flow to travel from the leading edge to the last downstream point of interest on the plate. The boundary layer requires longer to become fully developed because of the viscous processes. Under certain conditions when the testing time is very short, the steady-state conditions may not be reached. In these cases, an evaluation of experimental data requires the prediction of shear stress, heat transfer, and other parameters in the unsteady flow region.

In the present study, the shock-induced flow over a semi-infinite flat plate in an expansion tube is analyzed. A schematic representation of the operating cycle of an expansion tube is presented in figure 1. The apparatus is divided by two diaphragms into three sections. The driver section contains a gas at high pressure. The driven section contains the test gas, and the expansion section contains an accelerating gas at low pressure. The test model is located near the downstream end of the expansion section. The test region is the area labeled (5) in figures 1(a) and 1(e). Reference 1 should be consulted for more details on the operation of an expansion tube.

For quantitative evaluation of the boundary-layer quantities over the plate surface, nitrogen is considered to be in the test section, and helium and argon are considered to be in the accelerating section. The reason for using argon in the accelerating section is to obtain the effect of an accelerating gas with a larger molecular weight on the relaxation of the boundary layer.

The relaxation of the helium boundary layer and the argon boundary layer to the test-gas (nitrogen) boundary layer is analyzed by solving the time-dependent boundary-layer equations of species concentration, momentum, energy, and continuity, along with the equation of state for a binary gas mixture. The appropriate transport and thermodynamic properties for the perfect gas mixture are evaluated by employing the Monchick exponential repulsive potential. (See ref. 2.) The governing equations are treated in the transformed plane by using a conical similarity variable to obtain the self-similar solutions. The resulting set of coupled second-order nonlinear partial differential equations are solved by a line-relaxation technique which is a method that has been used extensively for elliptic problems. The governing boundary-layer equations employed herein, although parabolic in nature, require boundary conditions at the leading edge as well as at the interface because of a change in sign of the coefficient of the convection term in this region. This type of behavior has been termed "singular parabolic" by Gevrey (ref. 3) and Lam (ref. 4).

SYMBOLS

A	ratio of shock velocity to free-stream velocity, U_S/U_O
a	fraction of model length

$C = \frac{\mu\rho}{(\mu\rho)_w}$

C_{12}^*, A_{12}^* molecular thermal diffusion factor parameters

$c \equiv c_1$

c_1 mass fraction of heavy gas, ρ_1/ρ

c_2 mass fraction of light gas, ρ_2/ρ

c_f local skin-friction coefficient, $\frac{\tau_w}{\frac{1}{2}\left(\rho_w U_o^2\right)_{N_2}}$

c_p specific heat of mixture at constant pressure

c_v specific heat of mixture at constant volume

$D_1{}^T$ thermal diffusion coefficient of heavy gas

D_{12} binary coefficient of diffusion

F function

G Blasius shear function, $\phi(0,\beta)$

H dimensionless enthalpy difference, $\frac{h - h_w}{h_w}$

H_o dimensionless enthalpy difference behind the shock in free stream, $\frac{h_o - h_w}{h_w}$

H_G Blasius enthalpy function, $H(0,\beta)$

H_M Mirels enthalpy function, $H(1,\beta)$

h local enthalpy of mixture; also step size in numerical method

$\bar{h}_i = c_i h_i$ where $i = 1, 2$

h_o local enthalpy behind shock in free stream

J	thermal diffusion factor, $\left(D_1{}^T \frac{\partial T}{\partial \beta}\right) \Big/ T\mu$; also iteration parameter
k	thermal conductivity of mixture
M	Mirels shear function, $\phi(1,\beta)$
$\overline{M}$	molecular weight
M_s	shock Mach number
m	count of steps in α-direction
N_{Le}	Lewis number, $\frac{\rho D_{12} c_p}{k}$
N_{Pr}	Prandtl number, $\frac{c_p \mu}{k}$
N_{St}	Stanton number, $-q_w \Big/ \left[(\rho_w)_{N_2} U_o (c_p)_{N_2} (T_r - T_w)\right]$
n	count of steps in β-direction
p	pressure; also iteration parameter
q	heat-transfer rate
R	gas constant
R'	universal gas constant
$R_{w,x}$	Reynolds number, $\frac{\rho_w U_o x}{\mu_w}$
T	temperature, K
T_o	free-stream temperature in region between shock and interface
T_r	recovery temperature
T_{st}	stagnation temperature in free stream (having temperature T_∞)

T_1 temperature of gas in front of shock

T_∞ free-stream temperature in region between interface and expansion fan

t time, measured so that at $t = 0$ the shock wave is located at leading edge of plate

t' time, measured from the moment secondary diaphragm is ruptured

t^* time, measured so that at $t^* = 0$ the interface is located at leading edge of plate

$\bar{t}$ transformed time variable in Crocco plane, identical to t

U_o free-stream velocity

U_S shock velocity

u velocity component parallel to plate surface in boundary layer

$\bar{u} \equiv u(x,y,t)$

v velocity component normal to plate surface in boundary layer

$$v_1' = -D_{12} \frac{\partial \ln c_1}{\partial y} - \frac{D_1^T}{\rho c_1} \frac{\partial \ln T}{\partial y}$$

x distance from leading edge along plate in x,t coordinate system

x' distance from secondary diaphragm along center line of expansion tube

x^* distance from leading edge along plate in x^*,t^* coordinate system

$\bar{x}$ transformed distance variable in Crocco plane, identical to x or x^*

---

y normal distance from plate

α conical coordinate in MR limit, $\frac{x}{U_o t}$

α^* conical coordinate in BL limit, $\frac{x^*}{U_o t^*}$

$\alpha_{crit} = \frac{\theta}{\delta^*}$

β dimensionless velocity, $\frac{u}{U_o}$

$\Gamma \equiv \frac{c_{p,2}}{c_{p,1}} = \frac{\gamma_2}{\gamma_2 - 1} \frac{\gamma_1 - 1}{\gamma_1} \frac{\overline{M}_1}{\overline{M}_2}$

γ ratio of specific heats, $\frac{c_p}{c_v}$

$\overline{\gamma}$ dimensionless time in MR limit, defined by equation (A16)

$\overline{\gamma}^*$ dimensionless time in BL limit, $\frac{\rho_w U_o^2 t^*}{\mu_w}$

δ thickness of velocity boundary layer

$\delta^* = \int_0^e \left(1 - \frac{u}{U_o}\right) \frac{\rho}{\rho_e} dy$ where e denotes edge of boundary layer

η dimensionless y-coordinate

θ momentum thickness, $\int_0^e \left(1 - \frac{u}{U_o}\right) \frac{u\rho}{U_o \rho_e} dy$

$\lambda = c \frac{c_{p,1}}{c_{p,2}} + (1 - c)$

μ dynamic viscosity of mixture

ν kinematic viscosity of mixture

ρ density of mixture

τ shear stress

ϕ shear function defined by equation (A25)

$\overline{\phi}$ dimensionless shear stress defined by equation (A21)

Subscripts:

1	heavy gas
2	light gas
e	edge of boundary layer
max	maximum
N_2	evaluated for nitrogen
w	evaluated at wall

Abbreviations:

Ar	argon
BL	Blasius
He	helium
MR	Mirels
N_2	nitrogen

BACKGROUND

Several authors (refs. 4 to 19) have evaluated the various boundary-layer parameters for a shock tube having similar unsteady characteristics. References 5 to 14 are related to the problem of a boundary layer on the walls of a shock tube, whereas references 4 and 15 to 19 discuss the boundary layer on a semi-infinite flat plate which develops behind an advancing shock wave. This latter problem is relevant to the present study and will be discussed in more detail.

Trimpi and Cohen (ref. 6) used an integral method for calculating the laminar boundary layer for the entire flow in a shock tube. They integrated the boundary-layer equations in the direction normal to the wall bounding the flow. These equations were further transformed into a conically self-similar coordinate system. The resulting hyperbolic differential equations were solved by the method of characteristics utilizing an integral

technique at the discontinuities (contact surface, and so forth) in order that the characteristic solution may proceed across the discontinuities.

Mirels (ref. 8) and Ackroyd (ref. 14) used a shock-fixed coordinate system in which the boundary-layer flow is steady and similar solutions are valid. Although the shock-based coordinate system appears to be very appealing for the flow conditions which can be approximated mathematically by infinitely long walls, it does not facilitate the solution of the governing equations for the case of a shock moving over a sharp leading-edge plate. The solution obtained in the shock-fixed coordinate system for such a problem is valid only in the vicinity of the shock and cannot be expected to satisfy the boundary condition at the leading edge of the plate.

Cohen (ref. 9) analyzed the boundary layer developed by a centered expansion fan advancing into a stationary fluid by reducing the boundary-layer equations to similarity form by using the conical similarity variable, $\xi = 1 - \frac{x}{U_0 t}$. He obtained the three-term power-series expansions of the stream function and the enthalpy in terms of ξ (the distance behind the wave head) which are valid for small values of ξ only. Becker (ref. 10), using a numerical continuation procedure, was successful in extending Cohen's results for velocity and temperature profiles up to $\xi = 0.9$. Basically, Becker's continuation procedure requires taking an initial profile given at some ξ_* with which the new profile is computed at $\xi > \xi_*$. However, at the tail of the expansion wave ξ_0 where the derivatives of the free-stream quantities are discontinuous, the continued profile fails to satisfy the wall compatibility conditions for $\xi > \xi_0$. In order to overcome this difficulty, Becker added correction terms having proper asymptotic behavior far from the wall and approximating the correct result near the wave tail ξ_0. Uniqueness of the results obtained by the continuation procedure can be challenged immediately.

Stewartson (ref. 15) studied the fluid motion induced by the impulsive motion of a semi-infinite plate (with velocity U_0) in its own plane ($x > 0$) and found that for the region $0 \leq x \leq U_0 t$, two boundary conditions are needed at each end of the region because the sign of the convection term changes in this region. This sign change implies that small disturbances travel in both directions, $x/U_0 t$ increasing and $x/U_0 t$ decreasing. Therefore, the solution now depends on conditions at $x = 0$ and at $x = U_0 t$. The limiting behavior of the boundary-layer solution must be Blasius as x approaches 0 and Rayleigh as x approaches $U_0 t$. Lam (ref. 4) also arrived at the same conclusion in treating a more general problem of a shock moving past a semi-infinite plate (with the coordinate system fixed at the leading edge of the plate). He found that for this problem the Blasius profile must be used at $x = 0$ and the Mirels (ref. 7) solution must be specified at $x = U_0 t$, where U_0 is the velocity of the fluid in the free stream following the shock. In the limiting case of a weak shock, Stewartson's and Lam's problems are identical.

The complete boundary-layer problem on the wall of a shock tube also has similar characteristics. Once again two boundary conditions are needed both at $x = 0$ (diaphragm location) and at $x = U_0 t$ (the contact discontinuity) to complete the solution in the interaction region ($0 \leq x \leq U_0 t$). Gupta (ref. 12) and Ban and Kuerti (ref. 13) have used the Mirels (ref. 8) solutions at $x = 0$ and $x = U_0 t$ in treating this problem.

References 4 to 19, with the exception of Stewartson, have considered the transient boundary layers formed by the passage of a shock wave. Detailed literature relevant to the non-shock-induced time-dependent boundary layers may be found in references 20 and 21.

PROBLEM FORMULATION

Governing Equations

The two-dimensional time-dependent compressible laminar boundary-layer equations for a binary mixture have been taken as the flow-governing equations for the problem under consideration. These equations, including viscous, heat conducting, and diffusional effects are (see refs. 22 and 23):

Continuity of mass:

$$\frac{\partial \rho}{\partial t} + \frac{\partial}{\partial x}(\rho u) + \frac{\partial}{\partial y}(\rho v) = 0 \tag{1}$$

Continuity of species:

$$\rho\left(\frac{\partial c_1}{\partial t} + u\frac{\partial c_1}{\partial x} + v\frac{\partial c_1}{\partial y}\right) = -\frac{\partial}{\partial y}\left(\rho c_1 v_1'\right) \tag{2}$$

Conservation of momentum:

$$\rho\left(\frac{\partial u}{\partial t} + u\frac{\partial u}{\partial x} + v\frac{\partial u}{\partial y}\right) = \frac{\partial}{\partial y}\left(\mu\frac{\partial u}{\partial y}\right) \tag{3}$$

Conservation of energy:

$$\rho\left(\frac{\partial h}{\partial t} + u\frac{\partial h}{\partial x} + v\frac{\partial h}{\partial y}\right) = \mu\left(\frac{\partial u}{\partial y}\right)^2 - \frac{\partial q}{\partial y} \tag{4}$$

where v_1' in equation (2) and q in equation (4) are defined, respectively, as

$$v_1' = -D_{12}\frac{\partial \ln c_1}{\partial y} - \frac{D_1{}^T}{\rho c_1}\frac{\partial \ln T}{\partial y} \tag{5}$$

$$-q = k\frac{\partial T}{\partial y} + D_{12}\left[\rho\left(\bar{h}_1\frac{\partial \ln c_1}{\partial y} + \bar{h}_2\frac{\partial \ln c_2}{\partial y}\right) + \frac{D_1{}^T}{D_{12}}\left(\frac{\bar{h}_1}{c_1} - \frac{\bar{h}_2}{c_2}\frac{\partial \ln T}{\partial y}\right)\right] \tag{6}$$

The gas mixture is assumed to be ideal and calorically perfect; that is,

$$p = \rho RT = p_1 + p_2 = \rho T\left(c_1R_1 + c_2R_2\right) \tag{7}$$

$$h = \bar{h}_1 + \bar{h}_2 = c_1h_1 + c_2h_2 = T\left(c_1c_{p,1} + c_2c_{p,2}\right) \tag{8}$$

The rectilinear coordinate system chosen is fixed to the flat plate where x is the distance along the surface measured from the leading edge, and the dimension y is measured normal to the surface as shown in figure 2.

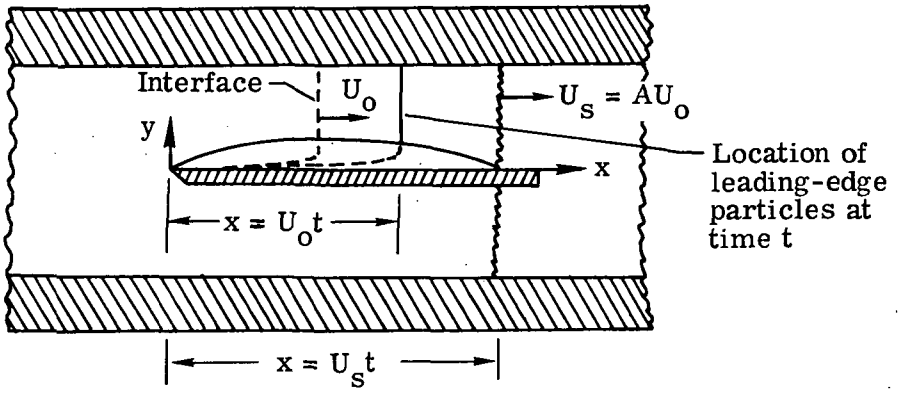

Figure 2.- Schematic diagram of flat-plate model showing the coordinate system used.

The following assumptions have been incorporated in this study:

(1) The flow external to the boundary layer is unaffected by the boundary-layer flow.

(2) The contact surface in the inviscid flow is assumed to be thin; therefore, no diffusion is allowed across the interface. This assumption is justified for a thin interface, that is, for the flow situations where the thickness of the interface is small compared with the length of the plate. Also, the relaxation of the boundary layer on the plate surface in the region where the Blasius state exists is not substantially affected by this restriction of zero-thickness interface because the approach to the Blasius value is asymptotic.

(3) For short-duration gas flows over solid boundaries having high values of conductivity and heat capacity per unit volume, the wall temperatures may be assumed to be constant. This assumption has been used consistently in this work.

Limitations Required for Conical Similarity

The inviscid flow in a shock or expansion tube is a function of the conical coordinate x'/t' as shown in figure 3. Since no viscous-inviscid interation is considered in the present analysis, the introduction of a flat plate alined with the stream at length ℓ from the secondary diaphragm does not alter the conical similarity of the inviscid flow. However, solution of the viscous flow over the flat plate requires specification of boundary conditions at the leading edge. Also, a time-similar flow may be specified if the coordinate system which originates at the leading edge is chosen. In this coordinate system the similar flow regions can now be specified. In a shock tube problem (x,t coordinate system), the flow between the shock and the interface is of interest. In this case the flow is invariant at constant x/t up to the time the interface crosses the leading edge of the model. However, for an expansion tube the flow of interest lies between the interface and the expansion fan. With the arrival of the interface, a new boundary-layer flow develops which again is time-similar if time is measured from the instant of arrival of the interface at the leading edge (x^*,t^* plane) provided a constant boundary condition can be specified at the interface $x^*/t^* = U_o$. In the general case, however, this condition is not possible since the interface traverses the shock-initiated flow in the x,t plane.

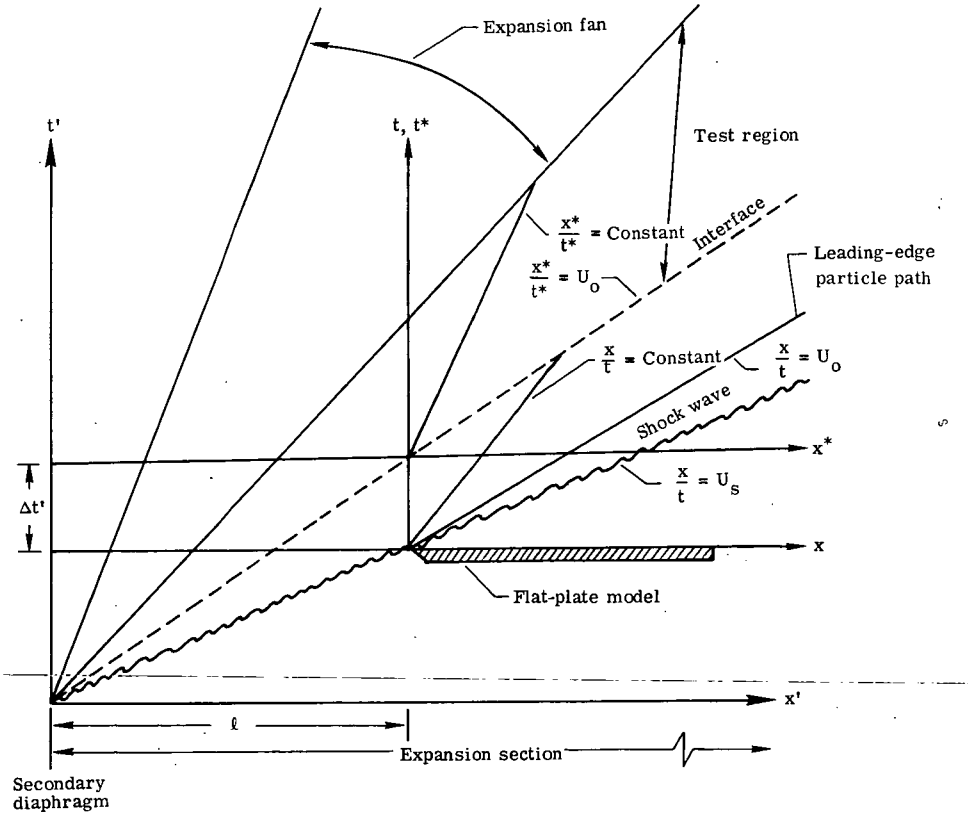

Figure 3.- Schematic representation of the test-section flow in distance-time plane.

(See fig. 3.) Since no general time-similar solution is possible, two limiting flow situations have been treated:

(1) If the interface arrives at the leading edge closely behind the shock wave, the time lag $\Delta t'$ may be taken as vanishingly small. The interface may be assumed to be coincident with the leading-edge particle line. (See fig. 4.) For this limit to be designated the MR (or Mirels) limit, the x,t plane may be conveniently used since the x,t and x^*,t^* planes now coincide.

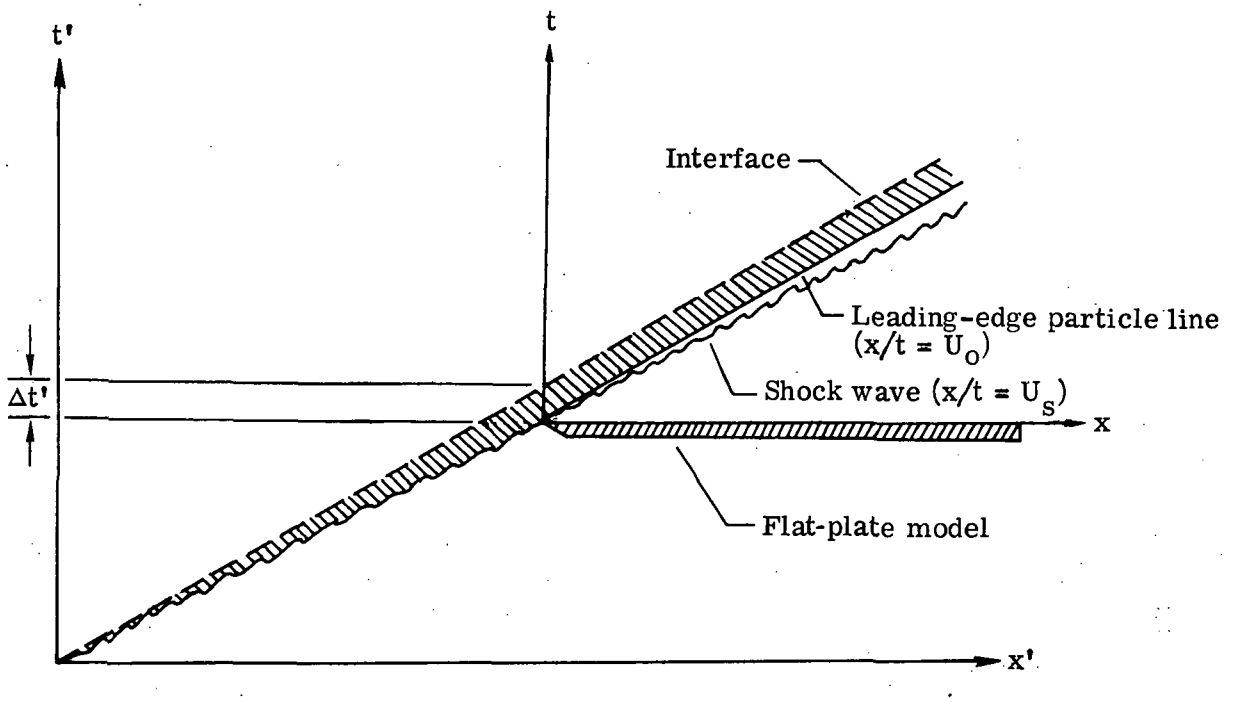

Figure 4.- Distance-time diagram for the MR limit. Time delay represented by the shaded region is assumed to be vanishingly small.

(2) On the other hand, if the shock wave is far ahead of the interface, that is, $\Delta t'$ approaches ∞, then the interface advances into a boundary layer which has almost completely relaxed to a steady-state (or Blasius) boundary layer. This limit, to be called the BL (or Blasius) limit, may conveniently be treated in the x^*,t^* plane (see fig. 5) after obtaining the fraction of the model length $\left(a = \frac{x}{U_o t}\right)$, from the x,t plane solutions; over this length the boundary layer behind the progressing shock wave may be assumed to be Blasius (BL). The value of a required to establish the BL limit may be obtained from a separate analysis similar to that by Cohen and Trimpi (ref. 6), Gupta (ref. 12), and Lam and Crocco (ref. 16). These analyses give the value of $a \approx 0.3$ for most of the flow conditions considered herein. It should be noted for this limit that with the arrival of the interface, the accelerating-gas Blasius boundary layer is disturbed and swept out by the test gas. A new Blasius boundary layer of the test gas now develops over a section of the model length near the leading edge.

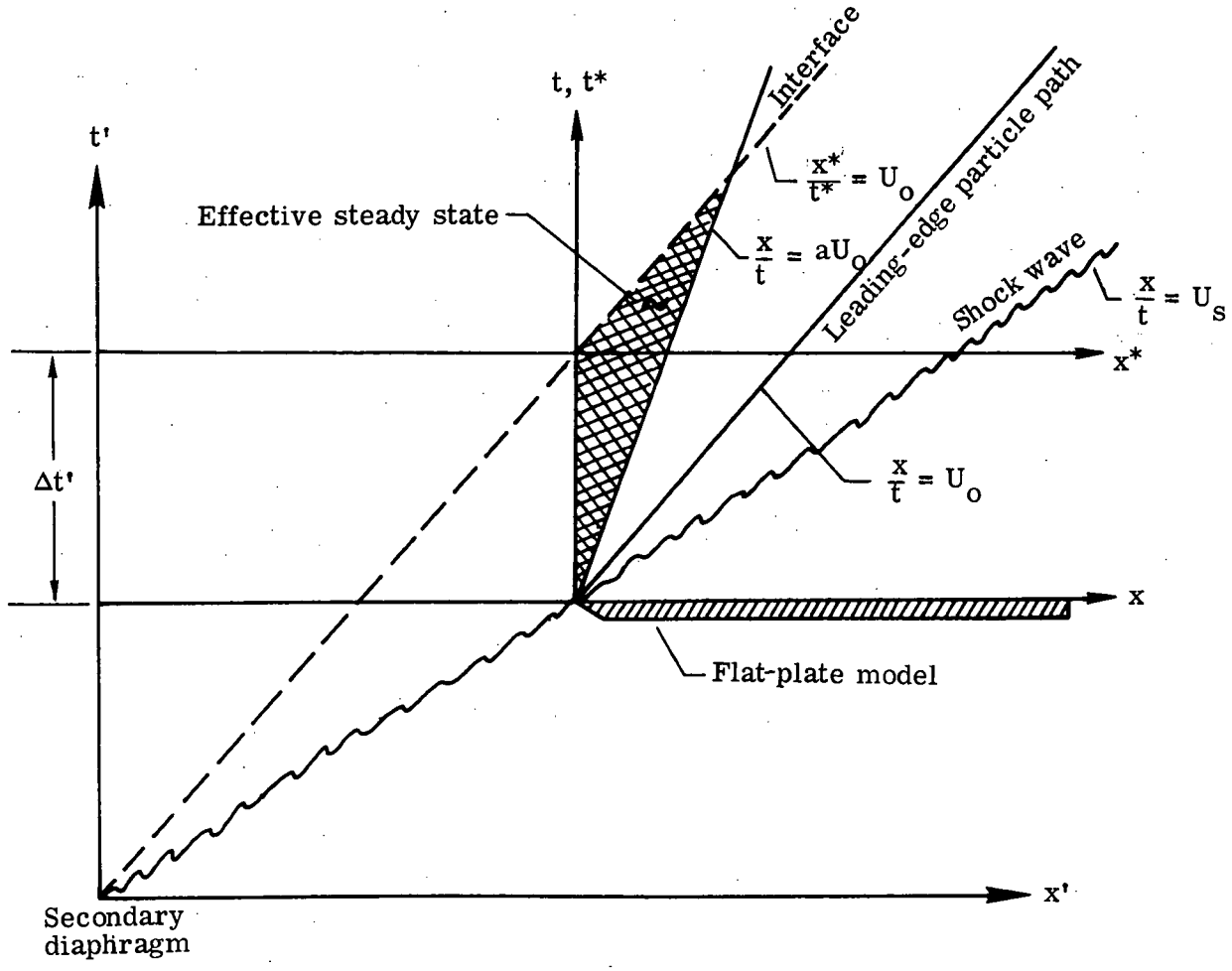

Figure 5.- Distance-time diagram for the BL limit.

Equations in Terms of Crocco's Conical Coordinates

Since the Crocco coordinates put the governing equations in a very compact form and have the distinct advantage over others in that the singular nature of the equations is more strongly evidenced, this system has been employed for the present problem. The other commonly used transformation for this type of problem is Stewartson's transformation. (See refs. 15 and 21.) However, the equations are quite cumbersome in this coordinate system. Moreover, the sign of the coefficient of convection term, which is both positive and negative so that propagation takes place in directions of α both increasing and decreasing, is not known until the velocity field is evaluated. This problem has been discussed in detail in reference 21.

The governing equations (2) to (4) are first transformed by using the Crocco system in which the independent variables are

$$\left.\begin{aligned} \bar{x} &\equiv x \\ \bar{u} &\equiv u(x,y,t) \\ \bar{t} &\equiv t \end{aligned}\right\} \tag{9}$$

and the dependent variables are

$$\left.\begin{aligned} c &= c(\bar{x},\bar{u},\bar{t}) \\ \tau &= \mu \frac{\partial u}{\partial y} = \tau(\bar{x},\bar{u},\bar{t}) \\ h &= h(\bar{x},\bar{u},\bar{t}) \end{aligned}\right\} \tag{10}$$

The independent variables (eqs. (9)) can be further recast (ref. 4) in the conical coordinate system. In this system the dimensionless independent variables are

$$\left.\begin{aligned} \alpha &= \frac{\bar{x}}{U_o \bar{t}} \\ \beta &= \frac{\bar{u}}{U_o} \\ \bar{\gamma} &= \frac{\rho_w U_o^2 \bar{t}}{\mu_w} \end{aligned}\right\} \tag{11}$$

and the dimensionless dependent variables are

$$\left.\begin{aligned} c(\alpha,\beta,\bar{\gamma}) &= c \\ \bar{\phi}(\alpha,\beta,\bar{\gamma}) &= \frac{\tau}{\rho_w U_o^2} \\ H(\alpha,\beta,\bar{\gamma}) &= \frac{h - h_w}{h_w} \\ H_1(\alpha,\beta,\bar{\gamma}) &= \frac{h_1 - h_w}{h_w} \end{aligned}\right\} \tag{12}$$

The conically self-similar solutions in the Crocco system can now be obtained if the following relations are specified for c, $\bar{\phi}$, H, and C:

$$\left.\begin{aligned} \frac{\partial c}{\partial \bar{\gamma}} &= 0 \\ \bar{\phi}(\alpha,\beta,\bar{\gamma}) &= \frac{\phi(\alpha,\beta)}{\sqrt{\alpha\bar{\gamma}}} \\ \frac{\partial H}{\partial \bar{\gamma}} &= 0 \\ \frac{\partial C}{\partial \bar{\gamma}} &= 0 \end{aligned}\right\} \tag{13}$$

Equations (2) to (4) with the use of expressions (9) to (13) finally become (see appendix A for details)

Continuity of species:

$$\phi^2 \frac{\partial}{\partial\beta}\left(\frac{N_{Le}}{N_{Pr}} \frac{\partial c}{\partial\beta} + J\right) + \phi \frac{\partial\phi}{\partial\beta}\left[\left(\frac{N_{Le}}{N_{Pr}} - 1\right)\frac{\partial c}{\partial\beta} + J\right] = C\alpha(\beta - \alpha)\frac{\partial c}{\partial\alpha} \tag{14}$$

Conservation of momentum:

$$\phi^2 \frac{\partial^2\phi}{\partial\beta^2} + \frac{C\beta}{2}\phi = \alpha(\beta - \alpha)\left(C\frac{\partial\phi}{\partial\alpha} - \frac{\partial C}{\partial\alpha}\right) \tag{15}$$

Conservation of energy:

$$\phi^2\left\{\frac{U_o^2}{h_w} + \frac{\partial}{\partial\beta}\left[\frac{1}{N_{Pr}}\frac{\partial H}{\partial\beta} + \frac{N_{Le} - 1}{N_{Pr}}(H_1 + 1)(1 - \Gamma)\frac{\partial c}{\partial\beta} + J(H_1 + 1)(1 - \Gamma)\right]\right\}$$

$$+ \phi \frac{\partial\phi}{\partial\beta}\left[\left(\frac{1}{N_{Pr}} - 1\right)\frac{\partial H}{\partial\beta} + (H_1 + 1)(1 - \Gamma)\left(\frac{N_{Le} - 1}{N_{Pr}}\frac{\partial c}{\partial\beta} + J\right)\right] = C(\beta - \alpha)\alpha \frac{\partial H}{\partial\alpha} \tag{16}$$

For the special case of a single-gas boundary layer ($c \equiv 1$), the terms containing N_{Le} and J are removed from the system.

The results presented in reference 24 indicate only a slight difference between the constant N_{Pr} and N_{Le} profiles and the variable N_{Pr} and N_{Le} profiles. Therefore, for simplicity N_{Pr} and N_{Le} will be assumed to be constant in the analysis with the values of 0.7 and 1.4, respectively. With constant N_{Le} and N_{Pr}, equations (14) to (16) reduce, after some algebraic manipulation, to

Continuity of species:

$$\frac{N_{Le}}{N_{Pr}}\phi^2 \frac{\partial^2 c}{\partial\beta^2} + \phi^2 \frac{\partial J}{\partial\beta} + \left(\frac{N_{Le}}{N_{Pr}} - 1\right)\phi \frac{\partial\phi}{\partial\beta}\frac{\partial c}{\partial\beta} + \phi \frac{\partial\phi}{\partial\beta} J = C\alpha(\beta - \alpha)\frac{\partial c}{\partial\alpha} \tag{17}$$

Conservation of momentum:

$$\phi^2 \frac{\partial^2\phi}{\partial\beta^2} + \frac{C\beta}{2}\phi = \alpha(\beta - \alpha)\left(C\frac{\partial\phi}{\partial\alpha} - \phi\frac{\partial C}{\partial\alpha}\right) \tag{18}$$

Conservation of energy:

$$\phi^2\left\{\frac{U_o{}^2}{h_w}+\frac{1}{N_{Pr}}\frac{\partial^2 H}{\partial\beta^2}+\frac{N_{Le}-1}{N_{Pr}}(1-\Gamma)\frac{\partial}{\partial\beta}\left[(H_1+1)\frac{\partial c}{\partial\beta}\right]+(1-\Gamma)\frac{\partial}{\partial\beta}\left[J(H_1+1)\right]\right\}$$

$$+\left(\frac{1}{N_{Pr}}-1\right)\phi\frac{\partial\phi}{\partial\beta}\frac{\partial H}{\partial\beta}+(1-\Gamma)\frac{N_{Le}-1}{N_{Pr}}(H_1+1)\phi\frac{\partial\phi}{\partial\beta}\frac{\partial c}{\partial\beta}+(1-\Gamma)(H_1+1)J\phi\frac{\partial\phi}{\partial\beta}$$

$$=C(\beta-\alpha)\alpha\frac{\partial H}{\partial\alpha} \tag{19}$$

where

$$(H_1+1)=(H+1)\frac{c_{p,1}/c_{p,2}}{c\left(\frac{c_{p,1}}{c_{p,2}}\right)+(1-c)}$$

BOUNDARY CONDITIONS

Definitions of Various Boundary-Layer Regions

The boundary-layer region in the BL limit may be divided in three parts (as shown in figs. 6 and 7):

(1) Shock region M:

$1 \leqq \alpha \leqq A$

$0 \leqq \beta \leqq 1$

$\overline{\gamma} \geqq 0$

$A = \frac{U_S}{U_O}$

This region was treated as suggested in references 4 and 16.

(2) Limited interaction region (LI) (between $\alpha^* = 1$ and $\alpha = 1$):

$(\alpha^* = 1) \leqq \alpha \leqq 1$

$0 \leqq \beta \leqq 1$

$\overline{\gamma} \geqq 0$

The limited interaction here implies that this region is part of the accelerating-gas interaction region ($0 \leqq \alpha \leqq 1$) which existed prior to the arrival of the interface. Therefore, this region is influenced by the leading edge of the flat plate, but not by the test-gas region

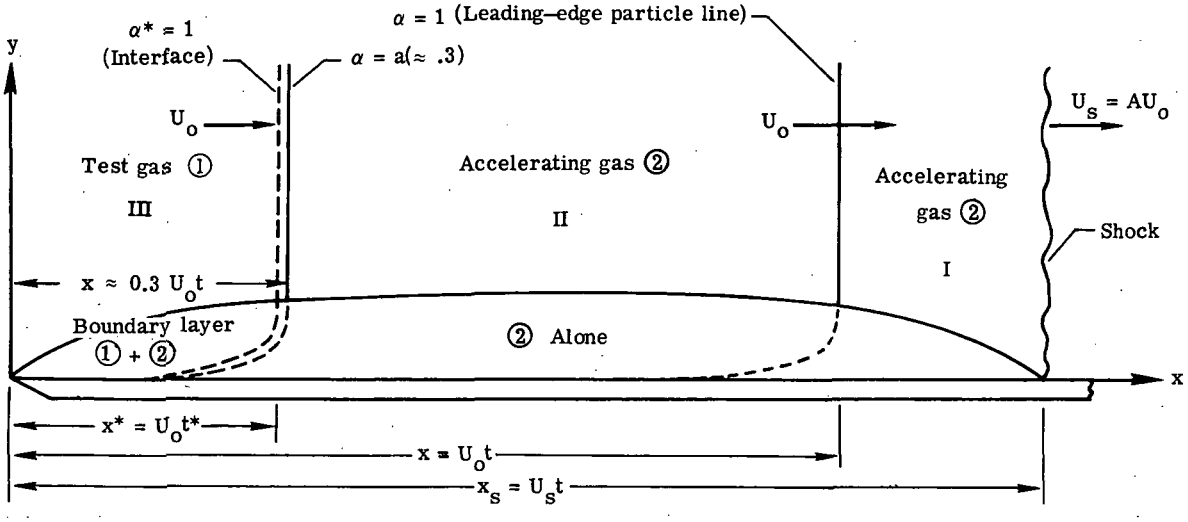

Figure 6.- Schematic representation of the flow field in the BL limit (physical plane).

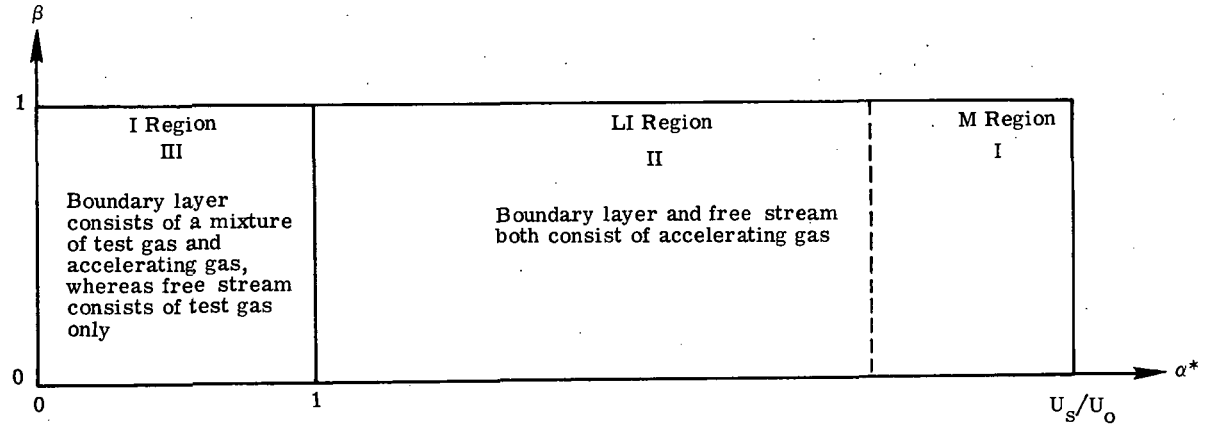

Figure 7.- Schematic representation of the flow field in the BL limit (α^*, β-plane).

which follows. The relaxation of this region, which occurs in a simple shock-initiated flow (such as in a shock tube) has been treated in references 4, 6, and 12. The analysis of reference 12 is used to define the "essentially steady-state" region and a value of $\alpha \approx 0.3$ is obtained for almost all the flow problems analyzed herein. The value $\alpha \approx 0.3$ should be a sufficient guideline for determining the essentially steady-state region. However, this value of α may be obtained with greater accuracy for a given flow problem by following the approach of reference 12.

(3) Interaction region I (close to the leading edge):

$0 \leqq \alpha^* \leqq 1$

$0 \leqq \beta \leqq 1$

$\overrightarrow{\gamma}^* \geqq 0$

The interaction region is bounded by two different steady-state flows. At the downstream boundary ($\alpha^* = 1$), the interface advances into a boundary layer of the accelerating gas which is assumed to have relaxed to the steady state since the BL limit treats only the situation where $\alpha^* = 1$ lies at $\alpha \leqq 0.3$. At the upstream boundary, $\alpha^* = 0$, a steady boundary layer in the test gas exists.

In the MR limit where the time interval between $\alpha = 1$ and $\alpha^* = 1$ line approaches zero, the boundary-layer region may be divided in two parts (see figs. 8 and 9):

(1) Shock region M:

$$1 \leqq \alpha \leqq A$$

$$0 \leqq \beta \leqq 1$$

$$\gamma \geqq 0$$

$$A = \frac{U_S}{U_O}$$

The treatment of this region is the same as in the BL limit.

(2) Interaction region I:

$$0 \leqq \alpha \leqq 1$$

$$0 \leqq \beta \leqq 1$$

$$\gamma \geqq 0$$

It should be noted that the limited interaction region LI in this limit is eliminated.

With the definitions of the two limiting situations for the flow field in α,β-plane given, attention will now be centered on specifying the boundary conditions.

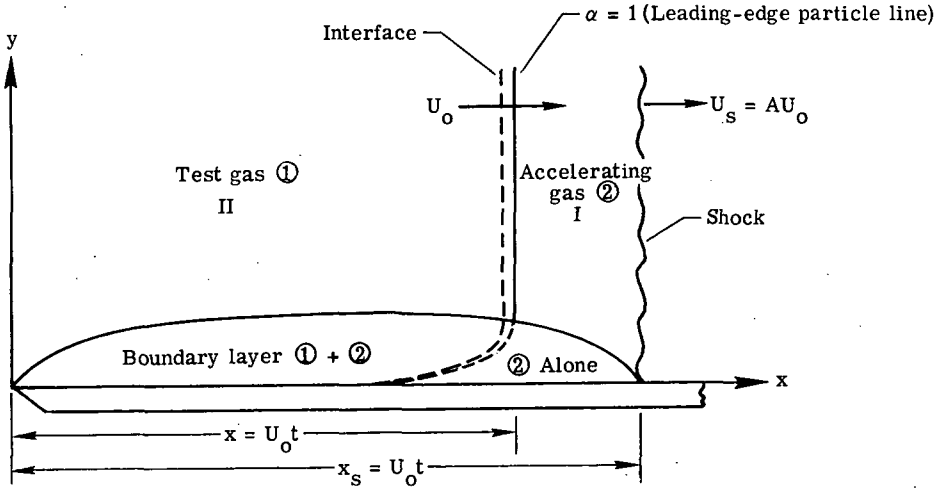

Figure 8.- Schematic representation of the flow field in the MR limit (physical plane).

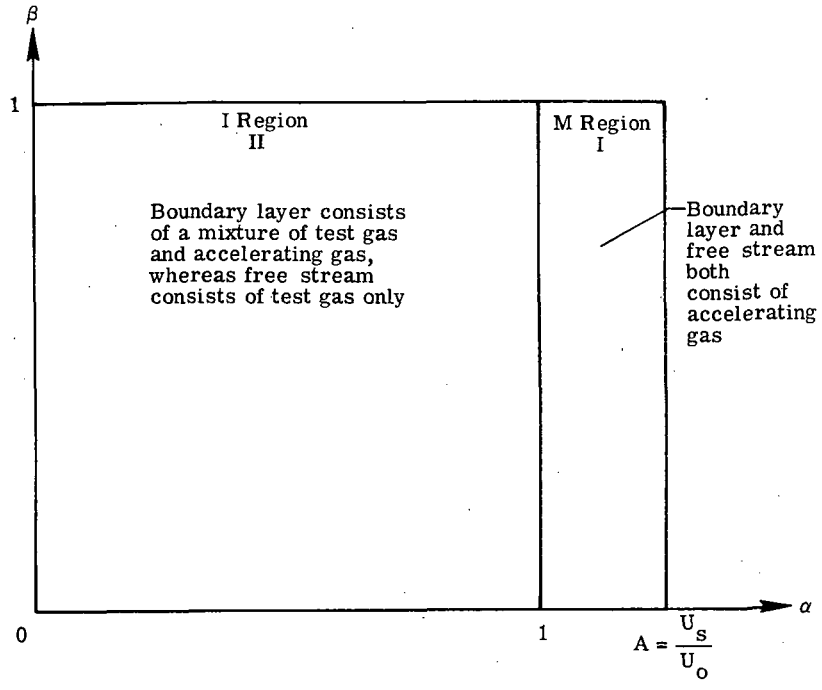

Figure 9.- Schematic representation of the flow field in the MR limit (α,β-plane).

Specification of Boundary Conditions

The objective here is to specify boundary conditions to solve equations (17) to (19) for c, ϕ, and H for $0 \leqq \beta \leqq 1$ for the appropriate α range in the two limits:

BL limit: $0 \leqq \alpha^* \leqq 1$

MR limit: $0 \leqq \alpha \leqq 1$

In both of these limits, ϕ and H must be given as functions of β near the leading edge ($\alpha \to 0$, $\alpha^* \to 0$) and at the boundaries of the shock region ($\alpha = 1$) and the limited interaction region ($\alpha^* = 1$). It may be noted that solutions for the BL and MR limits differ because of the different boundary conditions that are specified on ϕ and H at $\alpha^* = 1$ or $\alpha = 1$.

The boundary conditions will be specified in the following steps:

(1) Shock and limited interaction region boundary conditions: The shock and limited interaction region boundary conditions, needed for MR and BL limits, respectively, can be deduced from the same relations. First the shock region is considered. The solution in this region was established by Mirels (ref. 8) and Lam (ref. 4) and is briefly given as follows:

By letting

$$\phi(\alpha,\beta) = Q(\alpha)\, M(\beta)$$

and taking

$$Q(\alpha) = \sqrt{\alpha}\sqrt{\frac{A - 1}{A - \alpha}} \qquad (A > 1)$$

it is noted that for $\alpha = 1$, $\phi = M(\beta)$. Also, ϕ is real for $1 \leqq \alpha \leqq A$. This relationship also implies no shear stress definition for $\alpha > A$ (where there is no flow). Therefore, for $1 \leqq \alpha \leqq A$,

$$\phi(\alpha,\beta) = \sqrt{\alpha}\sqrt{\frac{A - 1}{A - \alpha}}\, M(\beta) \tag{20}$$

It may be noted that the shear stress $\phi \to \infty$ as $\alpha \to A$ which is expected because the boundary-layer thickness goes to zero near $\alpha = A$.

By assuming $H = H_M(\beta)$, it is noted that $C = C(H) = C(H_M) = C(\beta)$ for $1 \leqq \alpha \leqq A$. With the use of these assumptions and equation (20), equations (18) and (19) yield, respectively,

$$M \frac{\partial^2 M}{\partial \beta^2} + \frac{C}{2} \frac{A - \beta}{A - 1} = 0 \tag{21a}$$

$$M\left(\frac{1}{N_{Pr}} \frac{\partial^2 H_M}{\partial \beta^2} + \frac{U_o^2}{h_w}\right) - \frac{\partial M}{\partial \beta} \frac{\partial H_M}{\partial \beta}\left(1 - \frac{1}{N_{Pr}}\right) = 0 \tag{21b}$$

The boundary conditions on $M(\beta)$ and $H_M(\beta)$ are

$$\left.\begin{aligned} \left.\frac{\partial M}{\partial \beta}\right|_{\beta=0} &= 0 \\ M\big|_{\beta=1} &= 0 \end{aligned}\right\} \tag{22a}$$

$$\left.\begin{aligned} H_M(\beta = 0) &= 0 \\ H_M(\beta = 1) &= H_o = \frac{h_o - h_w}{h_w} \end{aligned}\right\} \tag{22b}$$

Equations (21a) and (21b) are the Mirels (ref. 8) similarity equations in terms of Crocco variables. To specify the shock region boundary condition on concentration, it should be noted that the boundary layer as well as the free stream consists of one gas (accelerating gas) in the region $1 \leqq \alpha \leqq A$. Therefore,

$$c(\alpha = 1,\beta) = 0 \tag{23}$$

for all values of β.

The limited interaction (LI) boundary conditions are recovered by setting $\alpha = -\alpha^*$ and $A = 0$ in equations (21) to (23). Here $A = 0$ does not imply the absence of flow, but merely that the momentum equation (21a) is to be solved for the Blasius value of the shear function. By setting $A = 0$ in equation (21a), it reduces to the form identical to that of Blasius equation (in Crocco form) that is to be developed in the next section.

(2) Leading-edge boundary conditions: The boundary condition at $\alpha^* = 0$ (BL limit) and at $\alpha = 0$ (MR limit) will be provided by the solution of the steady flat-plate governing equations. At $\alpha = 0$, $\phi = G(\beta)$; and, since any approach to the steady-state condition must be asymptotic, $\left.\frac{\partial \phi}{\partial \alpha}\right|_{\alpha=0} = 0$. The momentum equation (18) for such a case reduces to

$$G \frac{\partial^2 G}{\partial \beta^2} + \frac{C\beta}{2} = 0 \tag{24a}$$

Similarly, the assumption of a single gas boundary layer at $\alpha = 0$ and

$$H\big|_{\alpha=0} = H_G(\beta)$$

and

$$\left.\frac{\partial H}{\partial \alpha}\right|_{\alpha=0} = 0$$

simplify equation (19) to

$$G\left(\frac{1}{N_{Pr}} \frac{\partial^2 H_G}{\partial \beta^2} + \frac{U_o^2}{h_w}\right) - \frac{\partial G}{\partial \beta} \frac{\partial H_G}{\partial \beta}\left(1 - \frac{1}{N_{Pr}}\right) = 0 \tag{24b}$$

The boundary conditions on $G(\beta)$ and $H_G(\beta)$ are

$$\left.\begin{aligned} \left.\frac{\partial G}{\partial \beta}\right|_{\beta=0} &= 0 \\ G\big|_{\beta=1} &= 0 \end{aligned}\right\} \tag{25a}$$

$$\left.\begin{aligned} H_G(\beta = 0) &= 0 \\ H_G(\beta = 1) &= 0 \end{aligned}\right\} \tag{25b}$$

Under the assumption of an all test-gas boundary layer at $\alpha = 0$, the following concentration boundary condition may be specified for all values of β:

$$c(\alpha = 0, \beta) = 1 \tag{26}$$

The BL limit boundary conditions at $\alpha^* = 0$ can be obtained by replacing α by α^* in equations (24) to (26).

(3) Wall boundary conditions: In the MR limit boundary conditions on ϕ and H for a zero-slip, impermeable wall and constant wall temperature are

$$\left.\begin{aligned} &\frac{\partial \phi}{\partial \beta}(\alpha,\beta = 0) = 0 \\ &H(\alpha,0) = 0 \end{aligned}\right\} \qquad (0 \leqq \alpha \leqq 1) \qquad (27)$$

Since the plate surface represents a solid boundary, the following condition may be specified on c:

$$\frac{\partial c}{\partial \beta}(\alpha,\beta = 0) = 0 \qquad (0 \leqq \alpha \leqq 1) \qquad (28)$$

This condition means that there are no normal concentration gradients of either gas on the surface of the plate since the plate surface is neither a source nor a sink for either species.

The wall boundary conditions for the BL limit may be obtained from equations (27) and (28) by replacing α by α^*.

(4) Boundary-layer edge or free-stream condition: The free-stream boundary conditions on ϕ and H for the MR limit are

$$\left.\begin{aligned} &\phi(\alpha,\beta = 1) = 0 && (0 \leqq \alpha \leqq 1) \\ &H(\alpha,\beta = 1) = \frac{(h_w)_{N_2} - h_w}{h_w} && (0 \leqq \alpha \leqq 1) \end{aligned}\right\} \qquad (29)$$

In equations (29), the free-stream temperature has been taken equal to the plate temperature. Also, the free stream up to the contact surface will consist of all test gas. Hence,

$$c(\alpha,\beta = 1) = 1 \qquad (0 \leqq \alpha \leqq 1) \qquad (30)$$

Once again, the BL limit boundary conditions may be obtained by using α^* in place of α in equations (29) and (30).

The values of the parameters A, U_0^2/h_w, T_0/T_w, and so forth required in obtaining the boundary condition and for solving the governing equations have been obtained from the inviscid shock-tube relations (ref. 25). These relations are given in appendix B.

FLUID PROPERTIES

The fluid properties needed in the boundary-layer equations are ρ, c_p, c_v, μ, k, h_1, h_2, h, D_{12}, and $D_1{}^T$. The properties developed here are those dealing with binary mixtures of nonreacting gases. The binary mixtures considered are

(1) Nitrogen (test gas) and helium (the accelerating gas).

(2) Nitrogen (test gas) and argon (the accelerating gas).

The mixture properties are functions of the mass fraction of the individual species and properties of the pure species comprising the mixture. Extensive calculations for the required transport and thermodynamic properties have been made and these properties are discussed in appendix C. It should be mentioned that the binary collision integral $\Omega_{12}^{(1,1)^*}$ which appears in the various transport properties expressions depends on the choice of the molecular interaction potential. In this work this collision integral evaluated by Monchick's (ref. 2) exponential potential has been used. This potential is known to be the true qualitative form of the repulsive intermolecular potential at high temperatures. As pointed out by Monchick (ref. 2), it seems doubtful that a simple Lennard-Jones potential can be used over more than part of the temperature range of interest. A comparison between the various transport properties, calculated by using the exponential potential and the Lennard-Jones potential, is included in appendix C.

COMPUTING PROCEDURE AND APPLICATIONS

Numerical Solution of the Governing Equations

The boundary-value problem formulated in this analysis requires the solution of three coupled nonlinear partial differential equations (eqs. (17), (18), and (19)). Since it is necessary to specify boundary conditions both at the leading edge of the plate and at the interface, the present problem was solved by using the Gauss-Seidel line-relaxation method, a technique which is used in elliptic problems. (See ref. 26.)

To obtain the finite-difference equivalent of equations (17) to (19), the derivatives appearing in these equations are replaced by the following central difference approximations:

$$\left.\begin{aligned} \frac{\partial F}{\partial \alpha} &= \frac{F_{m+1,n} - F_{m-1,n}}{2h} + O(h^2) \\ \frac{\partial F}{\partial \beta} &= \frac{F_{m,n+1} - F_{m,n-1}}{2h} + O(h^2) \\ \frac{\partial^2 F}{\partial \beta^2} &= \frac{F_{m,n+1} - 2F_{m,n} + F_{m,n-1}}{h^2} + O(h^2) \end{aligned}\right\} \tag{31}$$

The finite-difference molecule is shown in figure 10.

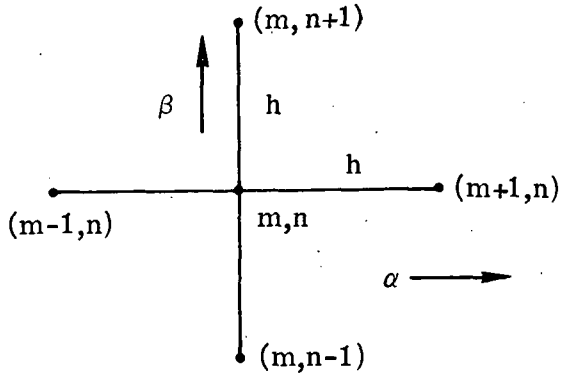

Figure 10.- Finite-difference molecule.

By using these finite-difference expressions, equations (17) to (19) may be written as follows for solution along lines of constant β. The superscript p refers to the iteration number.

$$\left[\frac{N_{Pr}}{N_{Le}}\frac{h}{4}\alpha_m(\alpha_m - \beta_n)\frac{C_{m,n}}{\phi^2_{m,n}}\right]c^p_{m-1,n} + c^p_{m,n} - \left[\frac{N_{Pr}}{N_{Le}}\frac{h}{4}(\alpha_m - \beta_n)\frac{C_{m,n}}{\phi^2_{m,n}}\right]c^p_{m+1,n}$$

$$= \frac{1}{2}\left(c^{p-1}_{m,n+1} + c^p_{m,n-1}\right) + \frac{1}{8}\left(1 - \frac{N_{Pr}}{N_{Le}}\right)\frac{\phi_{m,n+1} - \phi_{m,n-1}}{\phi_{m,n}}\left(c^{p-1}_{m,n+1} - c^p_{m,n-1}\right)$$

$$+ \frac{h}{4}\frac{N_{Pr}}{N_{Le}}\left(J^{p-1}_{m,n+1} - J^{p-1}_{m,n-1}\right) + \frac{h}{4}\frac{N_{Pr}}{N_{Le}}J^{p-1}_{m,n}\frac{\phi_{m,n+1} - \phi_{m,n-1}}{\phi_{m,n}} \tag{32}$$

$$\left[h\alpha_m(\alpha_m - \beta_n)\frac{C_{m,n}}{4\left(\phi^{p-1}_{m,n}\right)^2 - h^2 C_{m,n}\beta_n}\right]\phi^p_{m-1,n} + \phi^p_{m,n}$$

$$- \left[h\alpha_m(\alpha_m - \beta_n)\frac{C_{m,n}}{4\left(\phi^{p-1}_{m,n}\right)^2 - h^2 C_{m,n}\beta_n}\right]\phi^p_{m+1,n}$$

$$= -h\alpha_m(\alpha_m - \beta_n)\frac{\phi^{p-1}_{m,n}}{4\left(\phi^{p-1}_{m,n}\right)^2 - h^2\beta_n C_{m,n}}\left(C_{m+1,n} - C_{m-1,n}\right)$$

$$+ \frac{\left(\phi^{p-1}_{m,n}\right)^2}{2\left(\phi^{p-1}_{m,n}\right)^2 - \frac{h^2}{2}\beta_n C_{m,n}}\left(\phi^{p-1}_{m,n+1} + \phi^p_{m,n-1}\right) \tag{33}$$

$$\left[\frac{\alpha_m(\alpha_m - \beta_n)}{2h}\frac{C_{m,n}}{I_{m,n}}\right]H^p_{m-1,n} + H^p_{m,n} - \left[\frac{\alpha_m(\alpha_m - \beta_n)}{2h}\frac{C_{m,n}}{I_{m,n}}\right]H^p_{m+1,n}$$

$$= \frac{U_o^2}{h_w}\frac{\phi^2_{m,n}}{I_{m,n}} + \frac{1}{N_{Pr}h^2}\frac{\phi^2_{m,n}}{I_{m,n}}\left(H^{p-1}_{m,n+1} + H^p_{m,n-1}\right) + \left[\frac{N_{Le} - 1}{N_{Pr}}\frac{1 - \Gamma}{\Gamma}\frac{1}{4h^2}\frac{\phi^2_{m,n}}{\lambda_{m,n}}(c_{m,n+1} - c_{m,n-1})\right.$$

$$\left. + \left(\frac{1}{N_{Pr}} - 1\right)\frac{\phi_{m,n}}{4h^2}(\phi_{m,n+1} - \phi_{m,n-1}) + \frac{1 - \Gamma}{\Gamma}\frac{1}{2h}\frac{\phi^2_{m,n}}{\lambda_{m,n}}J_{m,n}\right]\frac{H^{p-1}_{m,n+1} - H^p_{m,n-1}}{I_{m,n}}$$

$$- \frac{1}{I_{m,n}}\left(I_{m,n} - \frac{2}{N_{Pr}}\frac{\phi^2_{m,n}}{h^2}\right) \tag{34}$$

In equation (34), $I_{m,n}$ is given by

$$I_{m,n} = \frac{2}{h^2 N_{Pr}}\phi^2_{m,n} - \frac{N_{Le} - 1}{N_{Pr}}\frac{1 - \Gamma}{\Gamma}\frac{1}{h^2}\frac{\phi^2_{m,n}}{\lambda_{m,n}}(c_{m,n+1} - 2c_{m,n} + c_{m,n-1}) - \frac{N_{Le} - 1}{N_{Pr}}\frac{1 - \Gamma}{\Gamma}$$

$$\times \frac{1}{4h^2}\frac{\phi_{m,n}}{\lambda_{m,n}}(c_{m,n+1} - c_{m,n-1})(\phi_{m,n+1} - \phi_{m,n-1}) + \frac{N_{Le} - 1}{N_{Pr}}\frac{(1 - \Gamma)^2}{\Gamma^2}\frac{1}{4h^2}$$

$$\times \frac{\phi^2_{m,n}}{\lambda^2_{m,n}}(c_{m,n+1} - c_{m,n-1})^2 + \frac{(1 - \Gamma)^2}{\Gamma^2}\frac{1}{2h}\frac{\phi^2_{m,n}}{\lambda^2_{m,n}}(c_{m,n+1} - c_{m,n-1})J_{m,n} - \frac{1 - \Gamma}{\Gamma}\frac{1}{2h}$$

$$\times \frac{\phi^2_{m,n}}{\lambda_{m,n}}(J_{m,n+1} - J_{m,n-1}) - \frac{1 - \Gamma}{\Gamma}\frac{1}{2h}\frac{\phi_{m,n}}{\lambda_{m,n}}(\phi_{m,n+1} - \phi_{m,n-1})J_{m,n} \tag{35}$$

Equations (32) to (34) have been uncoupled since only c^p, ϕ^p, or H^p at points (m-1,n), (m,n), and (m+1,n) is unknown in each of these equations, respectively. In addition, all nonlinearities have been removed by using values of the dependent variables from the previous iteration in the coefficients. Each of equations (32) to (34) forms a set of $\left(\frac{1}{h} - 1\right)$ simultaneous difference equations for a given value of n when m varies from 2 to 1/h. Since the coefficient matrix of each of these equations is of the tridiagonal form, the Thomas algorithm discussed in reference 26 provides a simple algorithm by which the solution may be obtained. To start the numerical solution, the mass-fraction is assumed to be unity throughout the flow field as if the problem to be analyzed contains the same gas in the accelerating section as in the test section. With $c \equiv 1$, equation (32) is identically satisfied. Next, after assuming an initial distribution of ϕ, equation (33) is solved by the Thomas algorithm along lines of constant β, beginning at the wall and

continuing until the outer boundary is reached. At this point the pth iteration has been completed. The iteration of the momentum equation is continued until

$$\text{Max}\left|\phi^{p} - \phi^{p-1}\right| < \epsilon_1$$

where ϵ_1 is of order of 10^{-5}. This value of p is referred to as p_{max}. With this solution to equation (33) and still assuming $c \equiv 1$, equation (34) is solved in the same manner p_{max} times. With the solutions to equations (33) and (34), equation (32) is now solved iteratively p_{max} times with appropriate boundary conditions. The resulting c-distribution is further used to improve the solutions for ϕ and H. This process is repeated until convergence to the desired accuracy

$$\left|\frac{\phi_w^J(\alpha,0) - \phi_w^{J-1}(\alpha,0)}{\phi_w^{J-1}(\alpha,0)}\right| < \epsilon_o$$

is obtained. Here ϵ_o is a small number taken as 10^{-5}. This criterion for convergence was selected since ϕ_w is a sensitive parameter characteristic of a solution. A similar criterion is used in reference 27.

In the present calculations $h = 0.01$ was used. To improve the convergence rate, the initial distributions were obtained by solving equations (32) through (34) for a coarse mesh ($h = 0.1$) and then with linear interpolation these coarse solutions served as initial guesses in the iteration with fine mesh ($h = 0.01$). This procedure significantly reduced the number of iterations needed for convergence to the desired accuracy. The procedure employed in the computer code is given in the flow chart (fig. 11).

Evaluation of Numerical Accuracy

The accuracy of the present numerical technique was evaluated by comparing with cases given by Lam (ref. 28). By assuming $c \equiv 1$ for a single-gas boundary layer and $C = 1$ for the viscosity law, equations (18) and (19) can easily be converted into the equations treated in reference 28 for a shock tube. The cases of reference 28 were computed by using the present numerical approach and a comparison is made in table I. There is very good agreement between the two results. It is thought that the present results are more accurate because of the use of double precision in the computations which has the effect of keeping the round-off errors to a minimum.

Boundary-Layer Parameters

For a binary mixture, heat transfer at the wall may be obtained from equation (6):

$$q_w = -\left[k_w\left(\frac{\partial T}{\partial y}\right)_w + \left(h_{w,1} - h_{w,2}\right)\left(\rho D_{12}\frac{\partial c}{\partial y} + \frac{D_1{}^T}{T}\frac{\partial T}{\partial y}\right)_w\right] \tag{36}$$

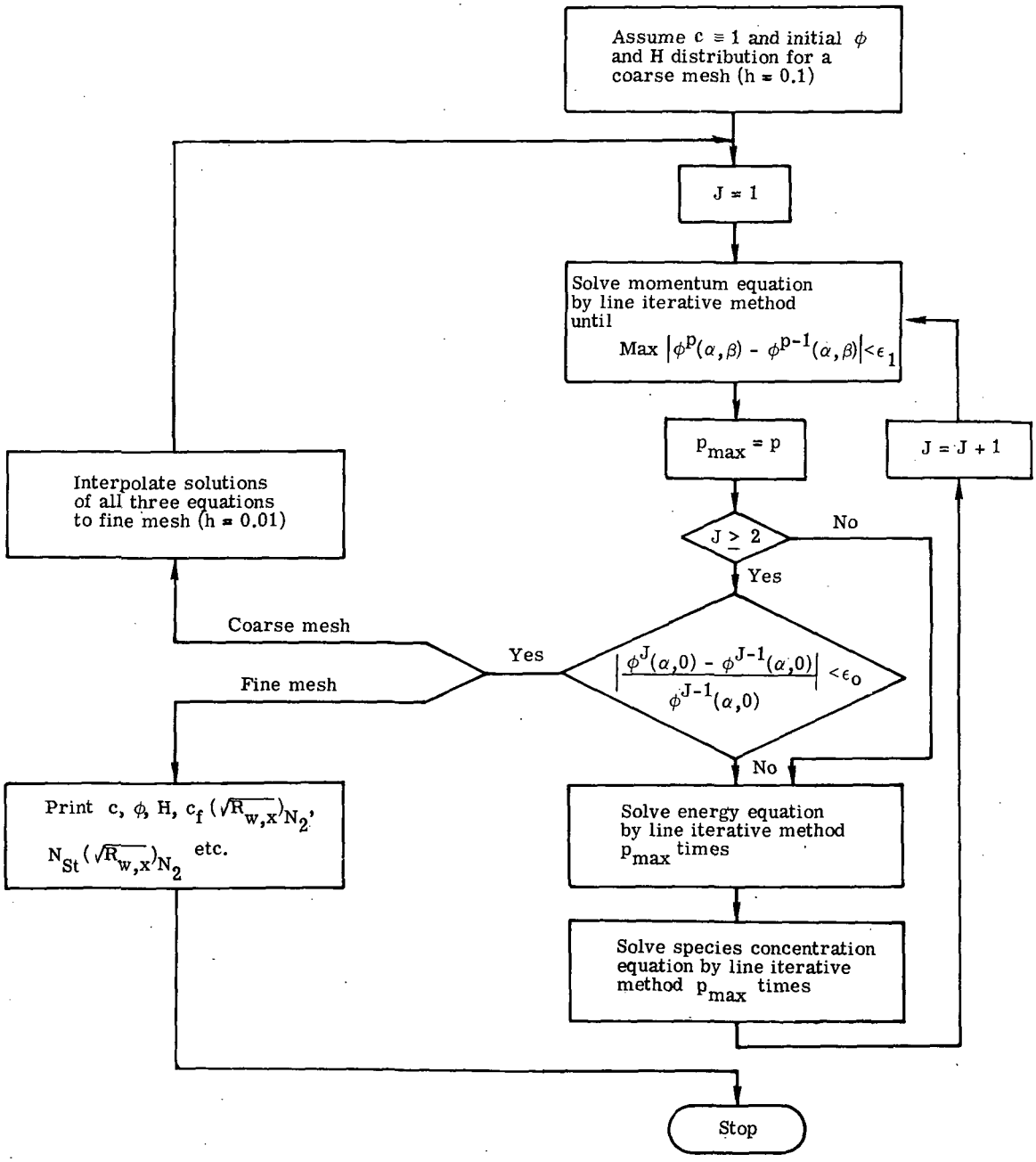

Figure 11.--Flow diagram for solving the coupled equations using a linearization scheme.

TABLE I.- COMPARISON OF SHEAR PARAMETER COMPUTED BY PRESENT NUMERICAL METHOD WITH THAT COMPUTED BY LAM (REF. 28)

[A = 1.2 and C = 1]

β	$\phi(\alpha,\beta)$ from Lam's results for –					$\phi(\alpha,\beta)$ from present results for –				
	$\alpha = 0$	$\alpha = 0.3$	$\alpha = 0.6$	$\alpha = 0.8$	$\alpha = 1.0$	$\alpha = 0$	$\alpha = 0.3$	$\alpha = 0.6$	$\alpha = 0.8$	$\alpha = 1.0$
0	0.330737	0.345968	0.517542	0.729052	1.145952	0.331981	0.340742	0.518983	0.736626	1.145524
.2	.328361	.341031	.496062	.697242	1.095612	.329971	.335141	.496927	.704008	1.095701
.4	.314174	.321737	.435211	.606915	.953981	.315757	.315419	.434982	.611645	.954121
.6	.274307	.277838	.338874	.462942	.727993	.275827	.272653	.338593	.465303	.728219
.8	.189752	.190712	.209048	.266147	.418522	.190831	.188173	.208274	.276861	.418886
.99	.0171208	.0171100	.0178980	.0177443	.0266531	.0181601	.0176282	.0177190	.0187913	.0274053

By introducing N_{Pr} and noting that

$$\frac{\partial F}{\partial y} = \frac{\phi}{\sqrt{\alpha\bar{\gamma}}} \frac{\rho_w U_o}{\mu_w} \frac{\partial F}{\partial \beta}$$

and

$$\left(\frac{\partial c}{\partial \beta}\right)_w = 0 \qquad \text{(for the present problem)}$$

from equation (36), after some algebraic manipulation,

$$q_w = - \frac{\rho_w U_o h_w \phi_w}{\sqrt{R_{w,x}}} \left[\frac{1}{N_{Pr}} \frac{\partial H}{\partial \beta} + \frac{1 - \Gamma}{c_w + (1 - c)\Gamma} J \right]_w \tag{37}$$

is obtained where

$$R_{w,x} = \frac{\rho_w U_o x}{\mu_w} = \alpha\bar{\gamma}$$

Equation (37) may now be used to obtain the following expression for the Stanton number:

$$N_{St} = \frac{\phi_w}{\left(\sqrt{R_{w,x}}\right)_{N_2} \left(\frac{T_r}{T_w} - 1\right)} \sqrt{\frac{\mu_w \rho_w}{(\mu_w \rho_w)_{N_2}}} \frac{h_w}{(h_w)_{N_2}} \left[\frac{1}{N_{Pr}} \frac{\partial H}{\partial \beta} + \frac{1 - \Gamma}{c + (1 - c)\Gamma} J \right]_w \tag{38}$$

In order to evaluate the recovery temperature T_r appearing in equation (38), a recovery factor is defined as follows:

$$r = \frac{T_r - T_\infty}{T_{st} - T_\infty} \tag{39}$$

where T_{st} is the stagnation temperature in the free stream (having a temperature T_∞) behind the interface. For the sake of simplicity, the recovery factor is assumed to be

related to the Prandtl number by

$$r = N_{Pr}^{1/2} \tag{40}$$

In the formulation, $T_\infty = T_w$ and

$$T_{st} = T_\infty + \frac{U_o^2}{2(c_p)_{N_2}}$$

Therefore, from equations (39) and (40)

$$\frac{T_r}{T_w} - 1 = N_{Pr}^{1/2} \frac{U_o^2}{2(h_w)_{N_2}} \tag{41}$$

Similarly, the expression for the local skin-friction coefficient may be obtained as

$$c_f = 2\sqrt{\frac{\rho_w \mu_w}{(\rho_w \mu_w)_{N_2}}} \frac{\phi_w}{\sqrt{(R_{w,x})_{N_2}}} \tag{42}$$

In the limit of an all N_2 boundary layer, c is identically equal to 1 and expressions (38) and (42) reduce to, respectively,

$$N_{St} = \frac{\phi_w}{\sqrt{(R_{w,x})_{N_2}}\left(\frac{T_r}{T_w} - 1\right)} \frac{1}{N_{Pr}} \left(\frac{\partial H}{\partial \beta}\right)_w \tag{43}$$

$$c_f = \frac{2\phi_w}{\sqrt{(R_{w,x})_{N_2}}} \tag{44}$$

From equations (41), (43), and (44), one can also write

$$\frac{N_{St}}{c_f} = \frac{(\partial H/\partial \beta)_w}{N_{Pr}^{3/2} \frac{U_o^2}{(h_w)_{N_2}}} \tag{45}$$

Results in Terms of Physical Variables

The obtained numerical results may further be utilized to examine the resulting behavior of the solution in terms of the physical variables. From the definition of the transformed variables,

$$\tau = \left(\frac{\rho_w U_o^3 \mu_w}{x}\right)^{1/2} \phi \tag{46}$$

or

$$\frac{\partial u}{\partial y} = \left(\frac{\rho_w U_o^3 \mu_w}{x}\right)^{1/2} \frac{\phi}{\mu}$$

so that

$$y(\alpha,\beta) = \left(\frac{x}{\rho_w U_o \mu_w}\right)^{1/2} \int_0^\beta \frac{\mu(\alpha,\xi)}{\phi(\alpha,\xi)}\, d\xi \tag{47}$$

Now

$$\mu = C\frac{\mu_w \rho_w}{\rho} = C\mu_w \rho_w \frac{R_1}{p_o}\frac{h}{c_p}\left[c + (1 - c)\frac{\overline{M}_1}{\overline{M}_2}\right] \tag{48}$$

where $1/\rho$ was obtained from equation (7), after rearrangement, and

$$\frac{h}{c_p} = \frac{h_{w,1}}{c_{p,1}} \frac{c_w + (1 - c_w)\dfrac{c_{p,2}}{c_{p,1}}}{c + (1 - c)\dfrac{c_{p,2}}{c_{p,1}}}(H + 1) \tag{49}$$

Hence, from equations (47), (48), and (49), the dimensionless ordinate is

$$\eta(\alpha,\beta) = \frac{y(\alpha,\beta)}{\left(\dfrac{x\mu_w\rho_w}{U_o}\right)^{1/2} \dfrac{\gamma_1 - 1}{\gamma_1}\dfrac{h_{w,1}}{p_o}} = \int_0^\beta \frac{\mu_R(\alpha,\xi)}{\phi(\alpha,\xi)}\, d\xi \tag{50}$$

where

$$\mu_R(\alpha,\xi) = C(\alpha,\xi)\left\{c(\alpha,\xi) + \left[1 - c(\alpha,\xi)\right]\frac{\overline{M}_1}{\overline{M}_2}\right\}$$

$$\times \left\{\frac{c(\alpha,0) + \left[1 - c(\alpha,0)\right]\dfrac{c_{p,2}}{c_{p,1}}}{c(\alpha,\xi) + \left[1 - c(\alpha,\xi)\right]\dfrac{c_{p,2}}{c_{p,1}}}\right\}(H + 1) \tag{51}$$

To evaluate the dimensionless ordinate $\eta\left(\alpha, \frac{u}{U_o}\right)$, the integral appearing in equation (50) is evaluated at fixed α for various β values by using Simpson's rule. This procedure gives profiles of $\eta\left(\alpha, \frac{u}{U_o}\right)$ at various α values which may be interpreted as velocity profiles $\frac{u}{U_o}(\eta)$ for various values of α.

From expression (50),

$$\frac{y}{\delta} = \frac{\eta}{\eta_\delta} = \frac{\int_0^\beta \left[\mu_R(\alpha,\xi)/\phi(\alpha,\xi)\right] d\xi}{\int_0^{0.99} \left[\mu_R(\alpha,\xi)/\phi(\alpha,\xi)\right] d\xi} \tag{52}$$

may also be written. The temperature in the boundary layer may be obtained from equation (49).

DISCUSSION OF RESULTS

Calculations of the mass fraction of test gas (nitrogen), skin friction, and heat-transfer coefficients for transient laminar boundary layer of a binary mixture of perfect gases on a flat plate in the interaction region of an expansion tube are presented in figures 12 to 15 for a wide range of shock Mach numbers. The gas considered in the test section is nitrogen. The gases considered in the expansion section are either helium, nitrogen, or argon. Helium has been most commonly used as the accelerating gas in expansion-tube tests. Nitrogen and argon are, however, considered (with the same free-stream velocity U_0) to determine the effect of molecular weight of the accelerating gas on the relaxation of the boundary layer. It should be noted that $M_S = 8.55$ in argon, $M_S = 7.17$ in nitrogen, and $M_S = 3$ in helium give the same free-stream velocity of 2.04 km/sec. In other cases considered, $M_S = 20.8$ in nitrogen and $M_S = 8$ in helium, both yield a free-stream velocity of 6.03 km/sec, whereas $M_S = 26.1$ in nitrogen and $M_S = 10$ in helium result in a velocity of 7.56 km/sec. Although the results for the higher Mach numbers are academic because of the assumptions made concerning the variation of properties of nitrogen at high temperatures, these calculations were performed in order to indicate trends. Thus, although nitrogen is treated as a perfect gas in the binary mixture, its viscosity is obtained from the real-gas values of Yos. (See ref. 29.)

In the present calculations, the plate surface was assumed to be at a constant temperature of 300° K and for convenience the free stream behind the interface was assumed to be at the same temperature. This last assumption is relevant for expansion-tube flow duplication but is inappropriate for simulation studies. (See ref. 30.) Perfect-gas relations, which are given in appendix B, were used to obtain the conditions behind the shock for a given shock Mach number in the accelerating gas.

Figure 12 shows distributions of the mass fraction of nitrogen between the flat-plate leading edge and the interface for various values of shock Mach number in different gases in the expansion section of the expansion tube for both the BL and MR limits. From these figures it may be concluded that the helium-nitrogen boundary layer has relaxed to the test gas (nitrogen) for values of α up to 0.3. For example, it relaxes to about 95.5 percent

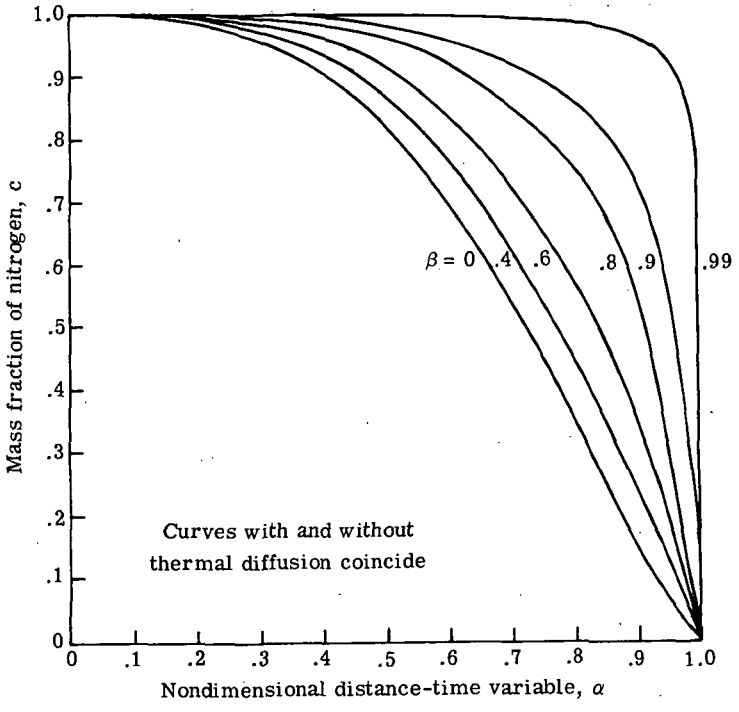

(a) $M_S = 3$ in helium; MR limit.

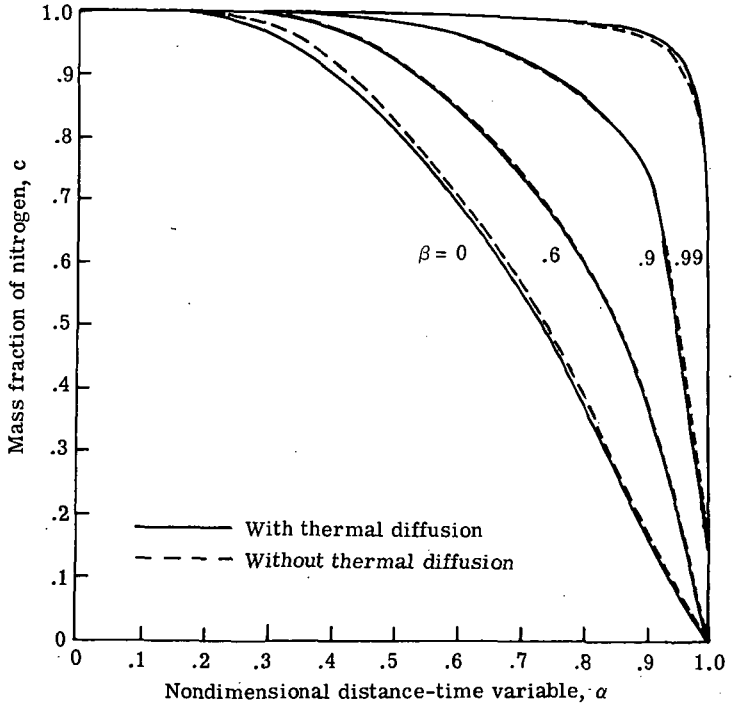

(b) $M_S = 8$ in helium; MR limit.

Figure 12.- Relaxation of mass fraction of nitrogen.

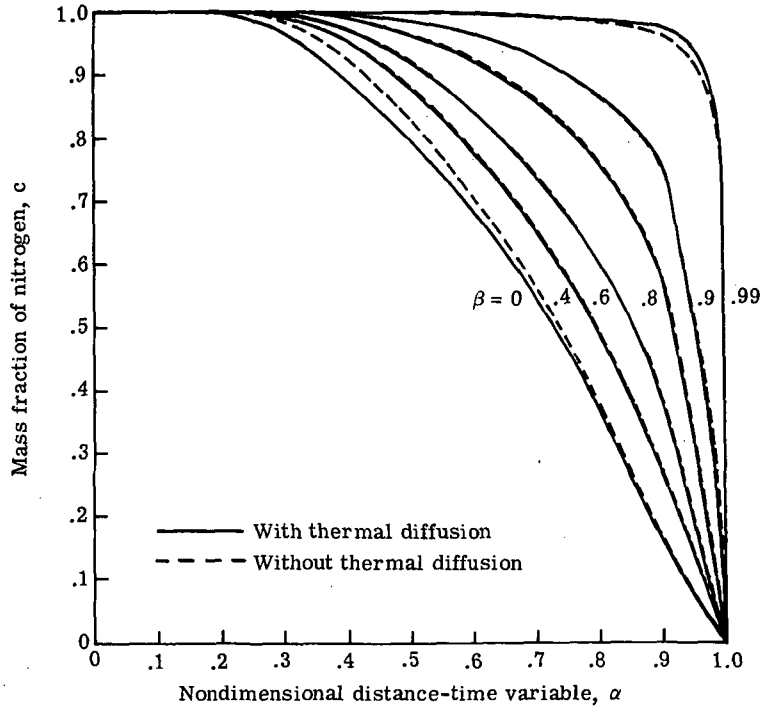

(c) M_s = 10 in helium; MR limit.

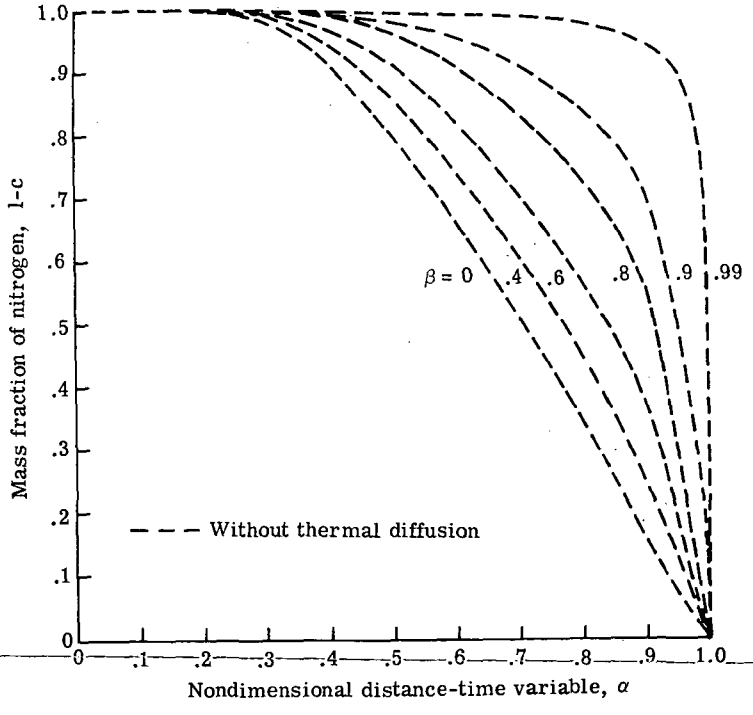

(d) M_s = 8.55 in argon; MR limit.

Figure 12.- Continued.

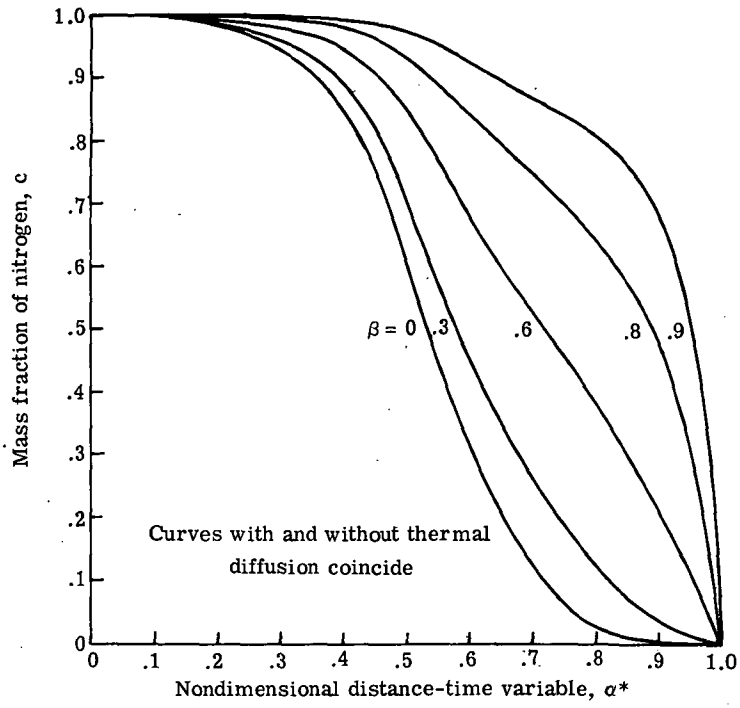

(e) $M_S = 3$ in helium; BL limit.

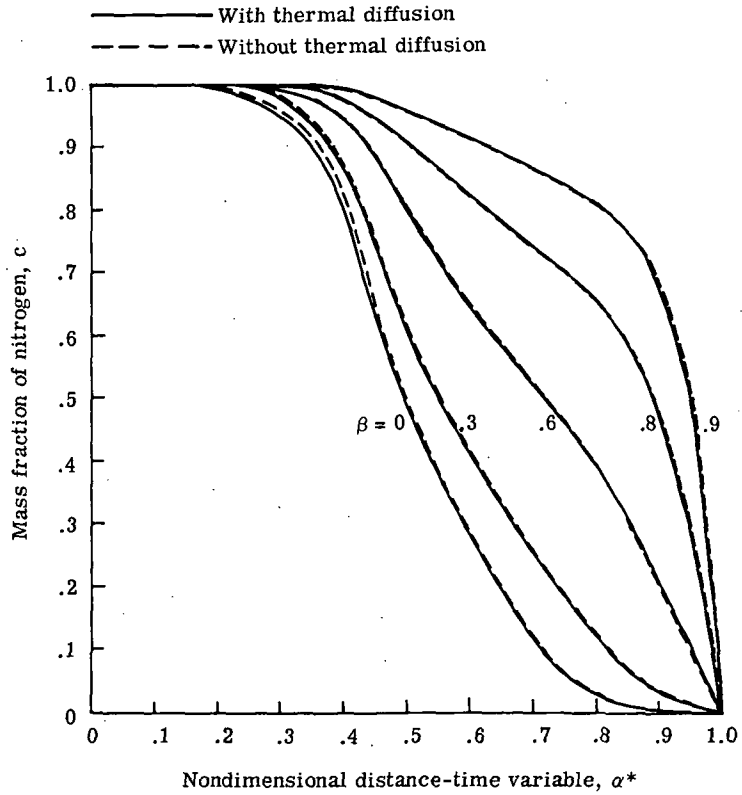

(f) $M_S = 8$ in helium; BL limit.

Figure 12.- Continued.

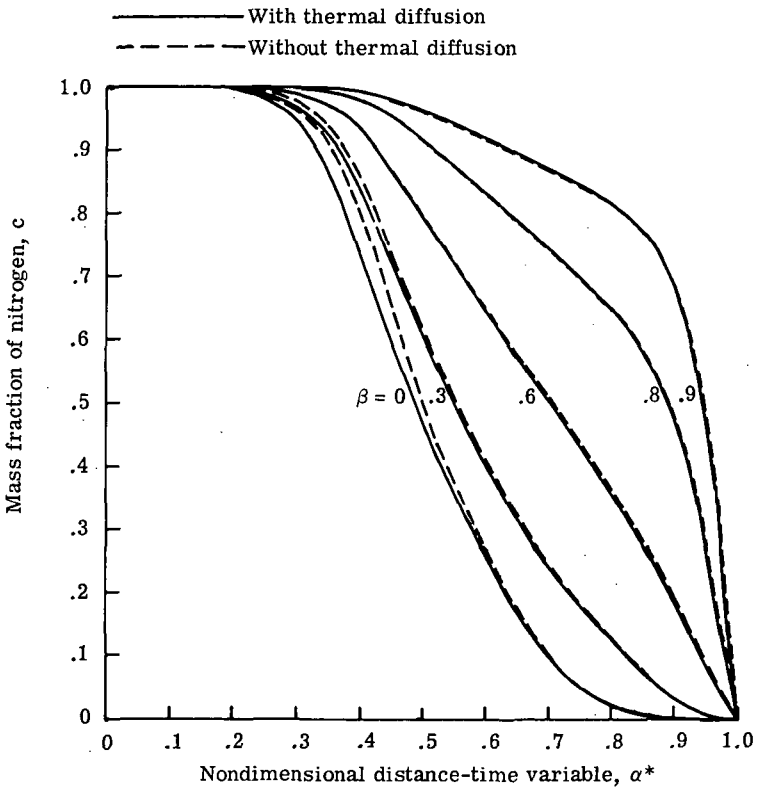

(g) M_S = 10 in helium; BL limit.

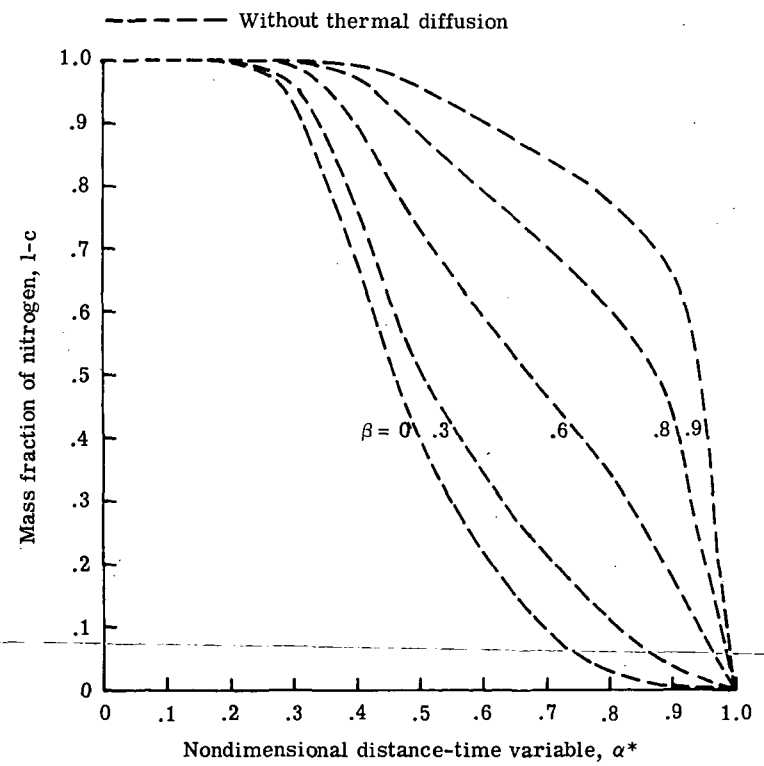

(h) M_S = 8.55 in argon; BL limit.

Figure 12.- Concluded.

nitrogen at the wall for $M_S = 3$ in helium, to 96.5 percent nitrogen at the wall for $M_S = 8$ in helium (with thermal diffusion), to 97 percent nitrogen at the wall for $M_S = 10$ in helium (with thermal diffusion); and to 98 percent nitrogen at the wall for $M_S = 8.55$ in argon. For the BL limit, these percentages are about 1 to 2 percent lower. These figures also indicate a physically plausible trend that the effect of thermal diffusion increases with the increase of shock Mach number. Figure 13 shows the relaxation of the binary boundary layer to a nitrogen boundary layer as the shock Mach number is increased. (The data points in this figure have been connected by straight lines.) It is revealed that the binary-gas boundary layer relaxes faster on the plate surface ($\beta = 0$) in terms of the parameter α (or α^*) as the shock Mach number in helium is increased from $M_S = 3$ to $M_S = 10$. This trend is consistent for the MR as well as the BL limits.

Figures 14(a) and 14(b) give the Stanton number distribution for the MR limit. Figure 14(a) also includes one curve (for $M_S = 3$ in helium) which gives the Stanton number (still multiplied by $\left(\sqrt{R_{w,x}}\right)_{N_2}$) for helium considered as the test gas. This figure indicates that for $\alpha \approx 0.3$, the Stanton number relaxes to within 6 percent of the steady-state nitrogen boundary-layer value. In figure 14(b) Stanton number distributions are compared for nitrogen (with $M_S = 26.1$) and helium (with $M_S = 10$) which have the same free-stream velocity U_O. This figure also indicates that for $\alpha \approx 0.3$, the Stanton number has relaxed to the steady-state nitrogen value (within about 9 percent). Also included in this figure is the curve for $M_S = 26.1$ in nitrogen when C (defining the viscosity law) is assumed to be unity. It may be noted from these solutions that when the gas used in the expansion section is a light gas (such as helium), the boundary layer relaxes faster to the steady-state test-gas condition. However, a different trend is indicated for the BL limit in figures 14(c) and 14(d). In this case a light accelerating gas results in a slower relaxation when compared with the other gases. A dip is noticeable in figure 14 for

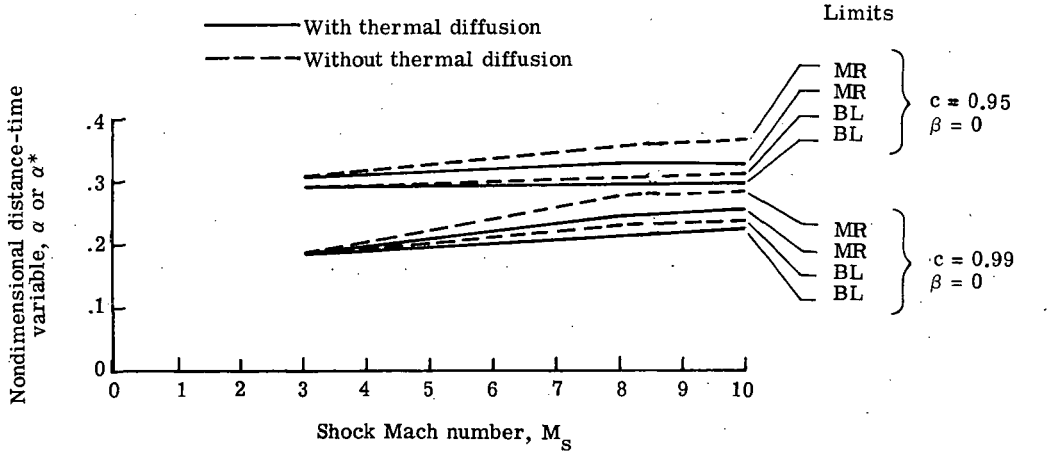

Figure 13.- Effect of shock Mach number on relaxation rate for nitrogen-helium boundary layer.

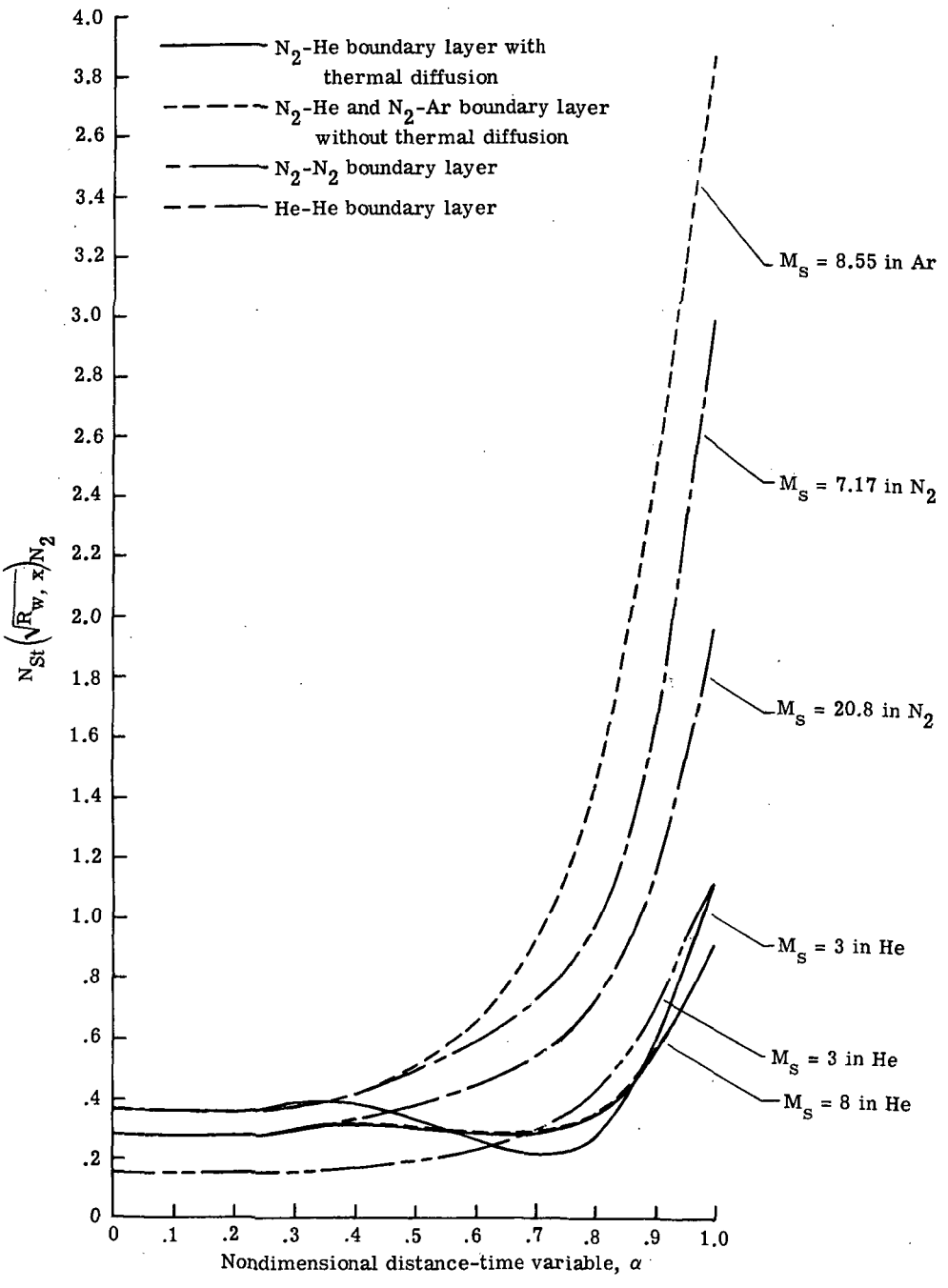

(a) M_S = 3, M_S = 8 in helium; M_S = 7.17, M_S = 20.8 in nitrogen; M_S = 8.55 in argon; MR limit.

Figure 14.- Stanton number distribution.

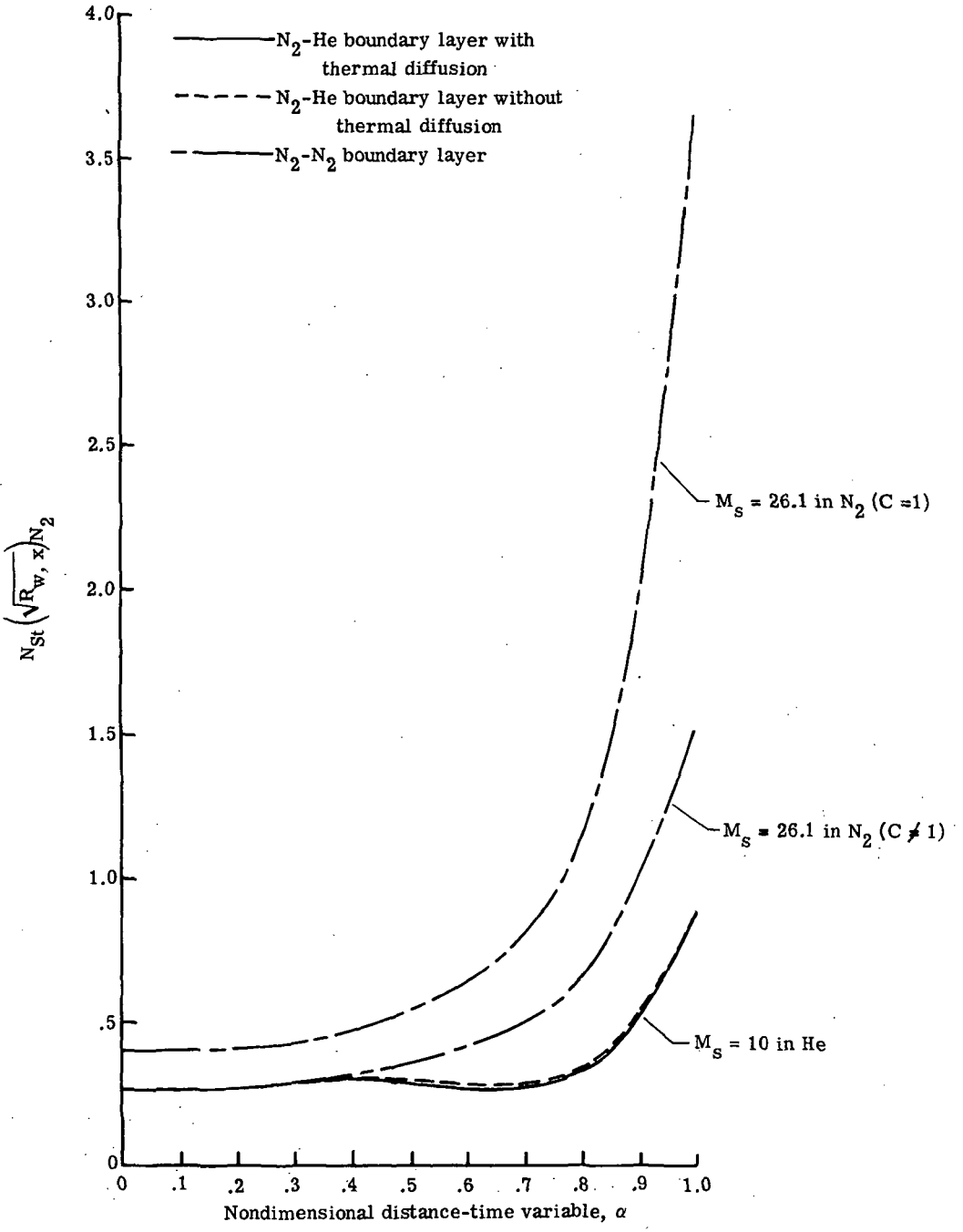

(b) M_s = 10 in helium; M_s = 26.1 in nitrogen; MR limit.

Figure 14.- Continued.

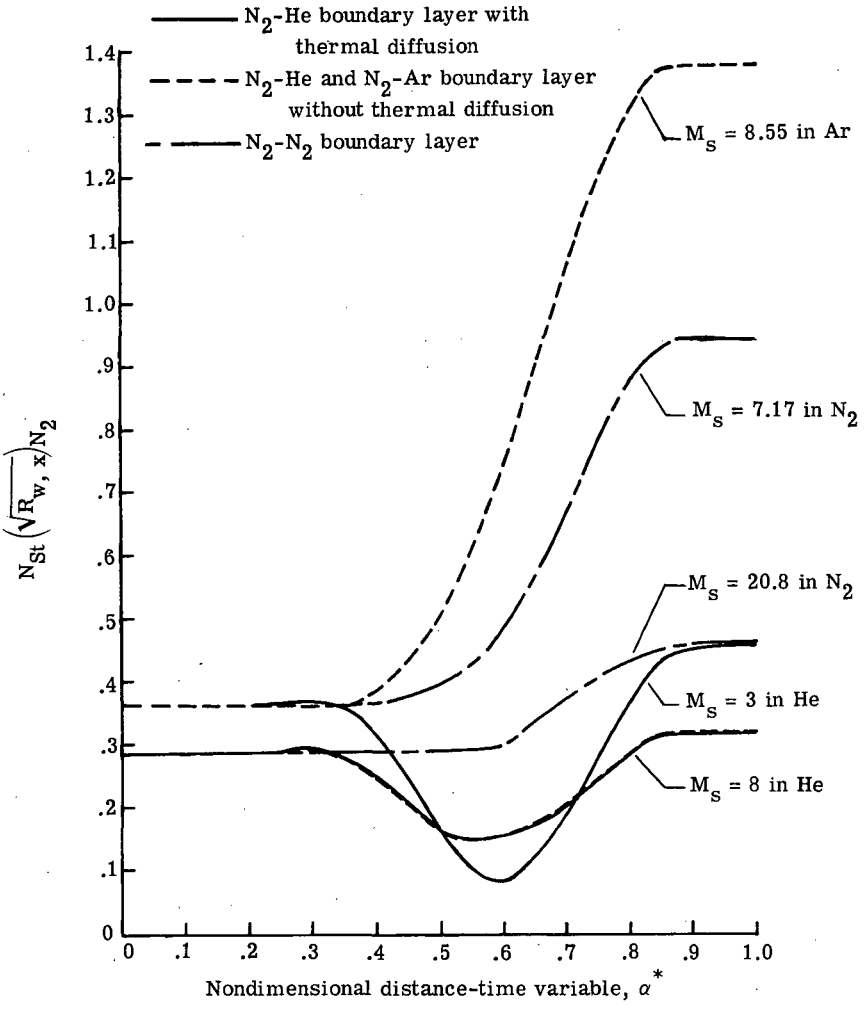

(c) $M_s = 3$, $M_s = 8$ in helium; $M_s = 7.17$, $M_s = 20.8$ in nitrogen; $M_s = 8.55$ in argon; BL limit.

Figure 14.- Continued.

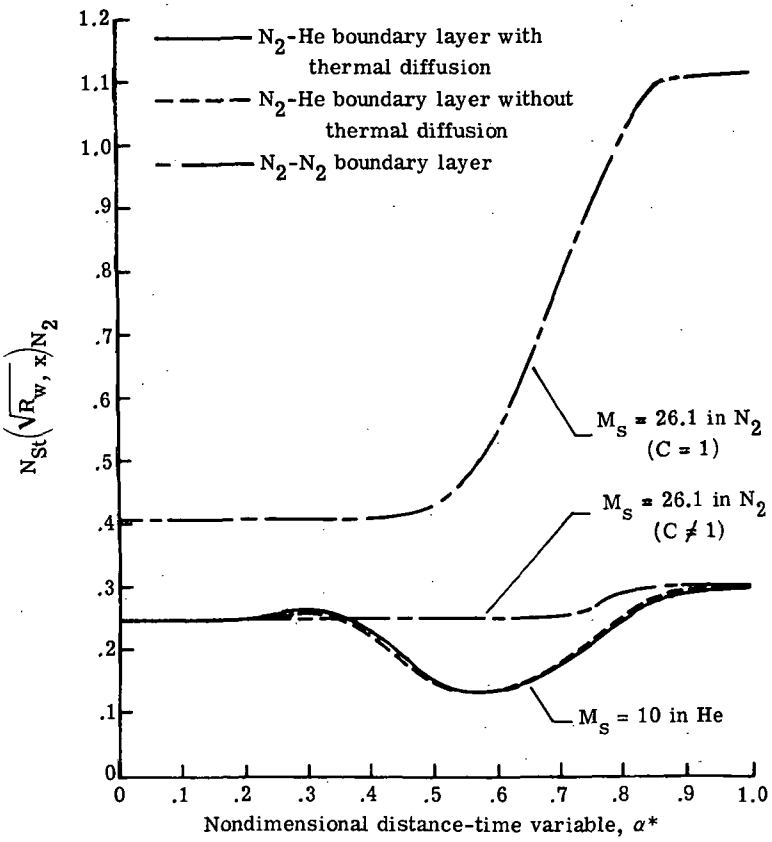

(d) M_s = 10 in helium; M_s = 26.1 in nitrogen; BL limit.

Figure 14.- Concluded.

cases when a lighter gas is used as the accelerating gas. The effect of thermal diffusion is less noticeable in the Stanton number distribution as compared with the nitrogen mass fraction distribution.

In figure 15, distributions of the local skin-friction coefficient are given for the MR and BL limits. In figures 15(a) and 15(b), which are for the MR limit, an interesting result is noted. These figures show that when helium is the accelerating gas, the skin-friction coefficient deviates only slightly from the steady-state value. This result may have significance in experiments since a faster instrumentation response to the steady-state value may be expected. For the other cases, $\alpha \approx 0.3$ is the location where the skin-friction coefficient has relaxed to within 5 percent of the steady-state skin-friction value in the test gas. The skin-friction coefficient for the case when helium is considered as the test gas (for $M_S = 3$ in helium) is also depicted in figure 15(a).

The skin-friction coefficient for the BL limit is shown in figures 15(c) and 15(d). In the BL limit, however, using the test gas as the accelerating gas appears to give faster relaxation. Once again, $\alpha^* = 0.3$ is the location on the plate surface upstream of which the skin-friction coefficient has relaxed to the test-gas steady-state value.

A qualitative comparison with the integral solutions of Trimpi and Cohen (ref. 6) for a shock tube using two different fluids can now be made. Their results show that for $\alpha < \alpha_{crit}$, most of the boundary layer is comprised of driver gas. This value of α_{crit} corresponds to $\alpha = 0.3$ obtained here. For a five- and six-term velocity profile, they found the value of 0.4 for α_{crit}. The comparison is approximate because the integral results do not give the exact extent of the driver-gas boundary layer.

Figures 16 to 18 give the distribution of velocity, temperature, and mass fraction of nitrogen, respectively, through the boundary layer as a function of the physical variable y/δ. The results presented in these figures are for $M_S = 8$ in helium in the MR limit. The velocity profiles are smooth and validate the assumption implicit in the Crocco transformation that $u(x,y,t)$ is a monotonically increasing function of y through the boundary layer. The velocity profiles at $\alpha = 0$ and $\alpha = 1$ are the self-similar Blasius and Mirels (ref. 8) profiles, respectively.

It should be noted here that δ represents the velocity boundary-layer thickness, evaluated by assuming that the edge of the velocity boundary layer is at $\beta = 0.99$ (that is, at the point where the velocity is 99 percent of the free-stream value). The thermal and the concentration boundary-layer thicknesses will be much larger and may be evaluated by using the value of β much closer to 1 (for example, $\beta = 0.999$).

Finally, figure 19 gives the relaxation of transformed boundary-layer thickness from Mirels' value at $\alpha = 1$ in helium (for $M_S = 8$) to the Blasius value at $\alpha = 0$ in nitrogen. Once again, only the MR limit result is shown. A rapid steepening of the η_δ

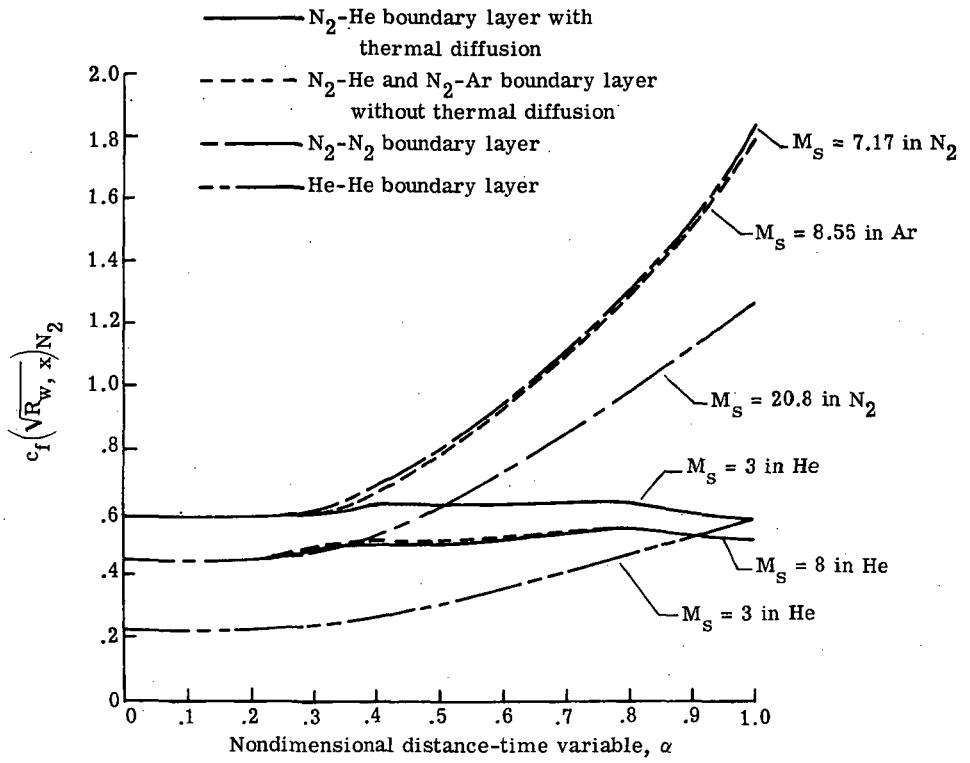

(a) $M_s = 3$, $M_s = 8$ in helium; $M_s = 7.17$, $M_s = 20.8$ in nitrogen; $M_s = 8.55$ in argon; MR limit.

Figure 15.- Distribution of local skin-friction coefficient.

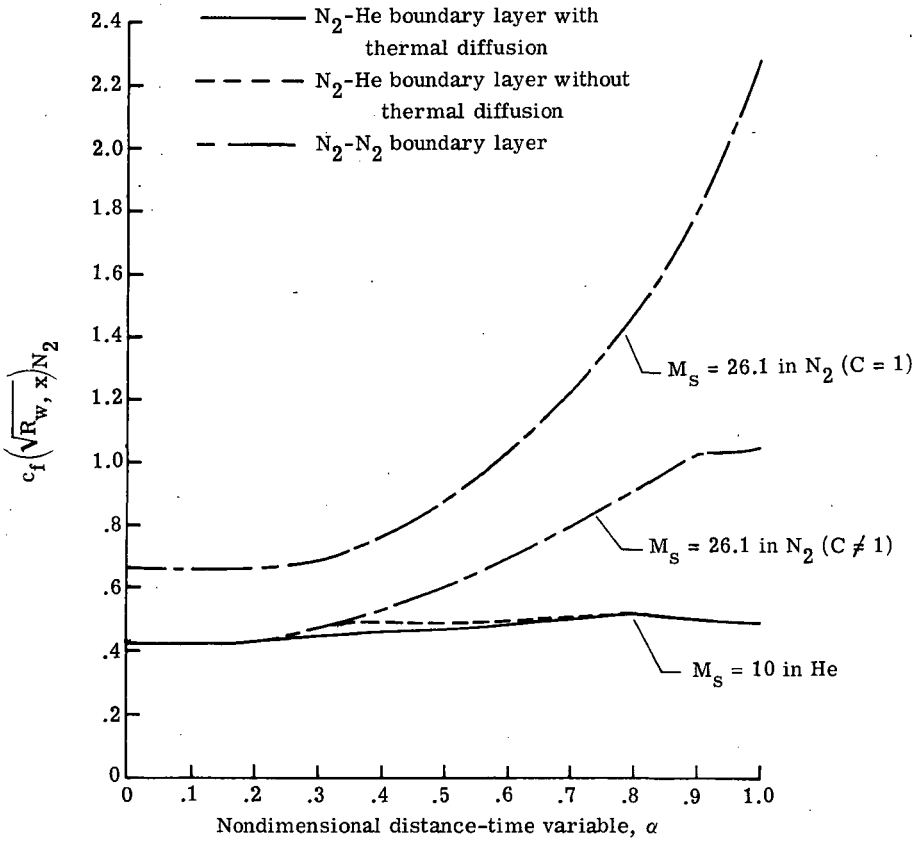

(b) M_s = 10 in helium; M_s = 26.1 in nitrogen; MR limit.

Figure 15.- Continued.

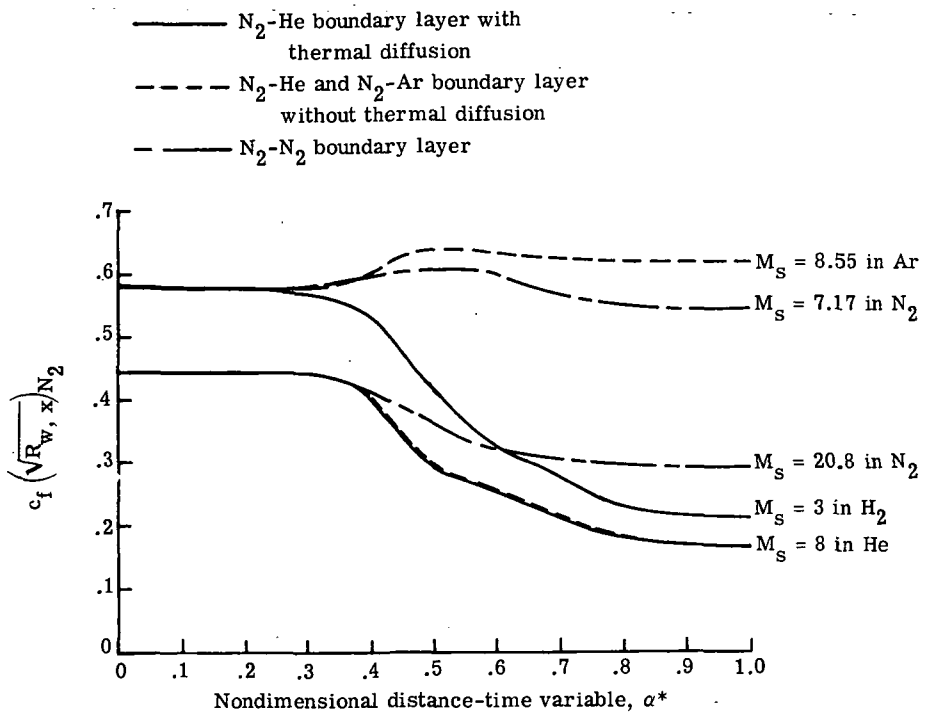

(c) $M_s = 3$, $M_s = 8$ in helium; $M_s = 7.17$, $M_s = 20.8$ in nitrogen; $M_s = 8.55$ in argon; BL limit.

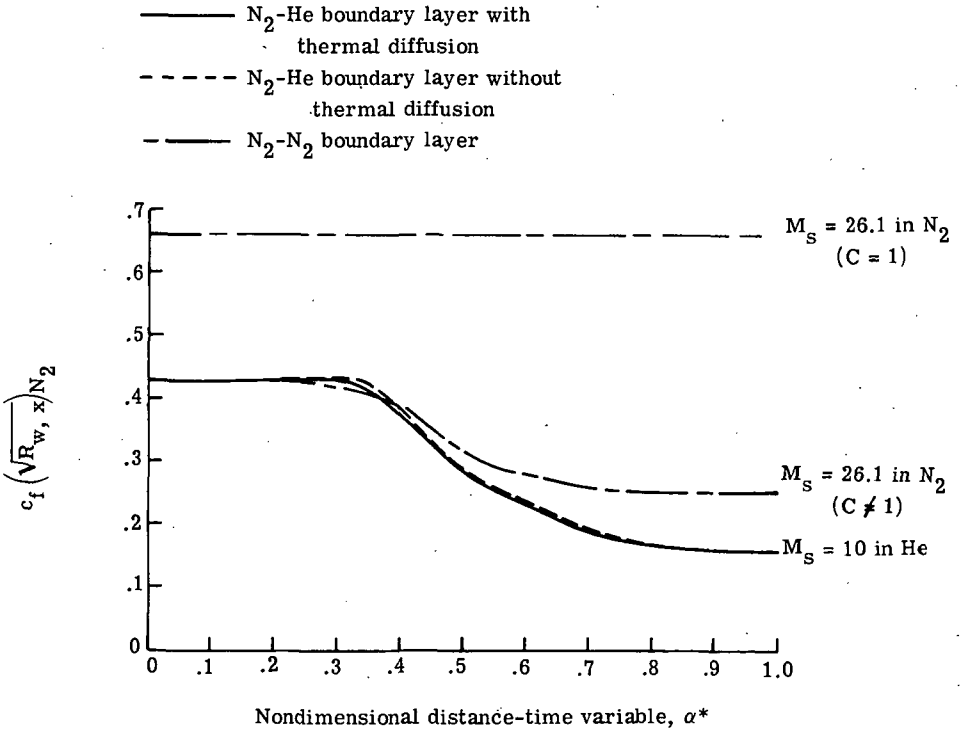

(d) $M_s = 10$ in helium; $M_s = 26.1$ in nitrogen; BL limit.

Figure 15.- Concluded.

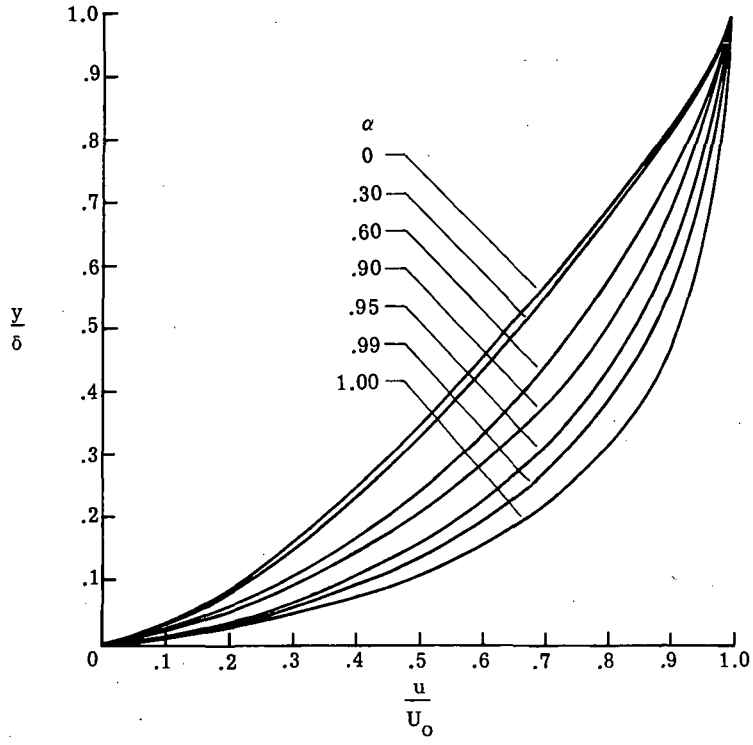

Figure 16.- Velocity distribution through the boundary layer for $M_s = 8$ in helium. MR limit.

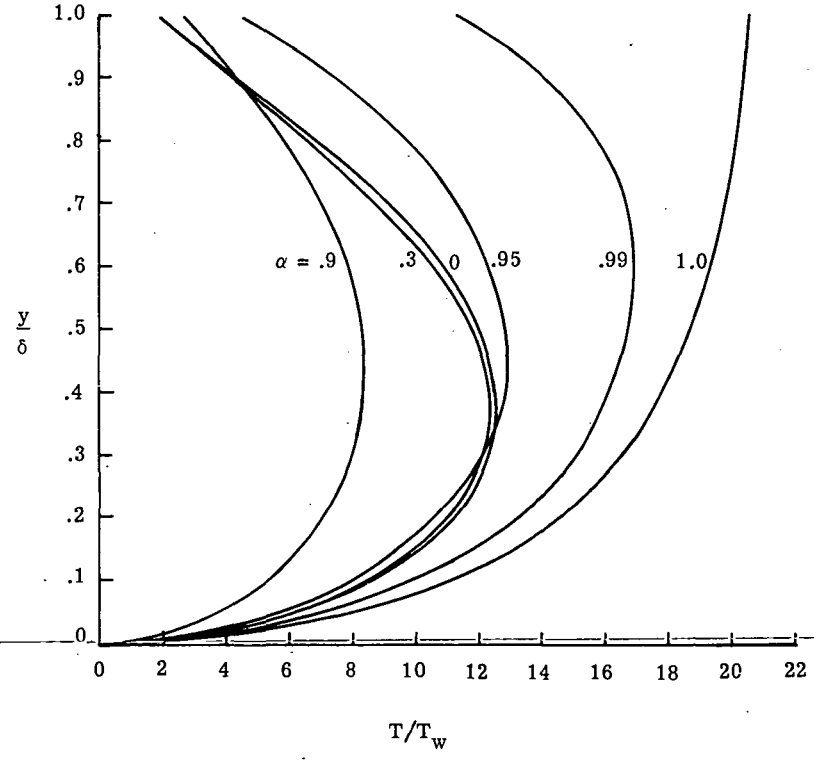

Figure 17.- Temperature distribution through the boundary layer for $M_s = 8$ in helium. MR limit.

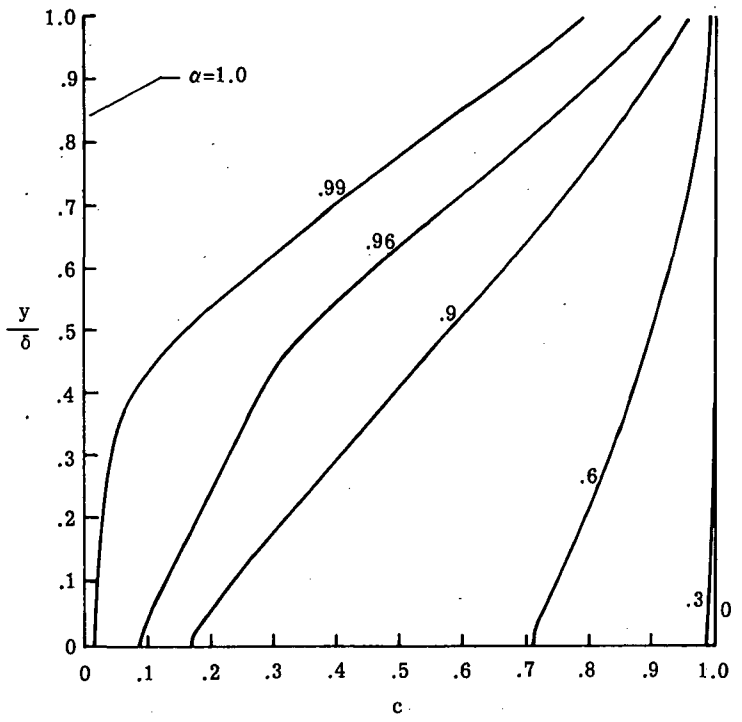

Figure 18.- Mass fraction of nitrogen through the boundary layer for $M_S = 8$ in helium. MR limit.

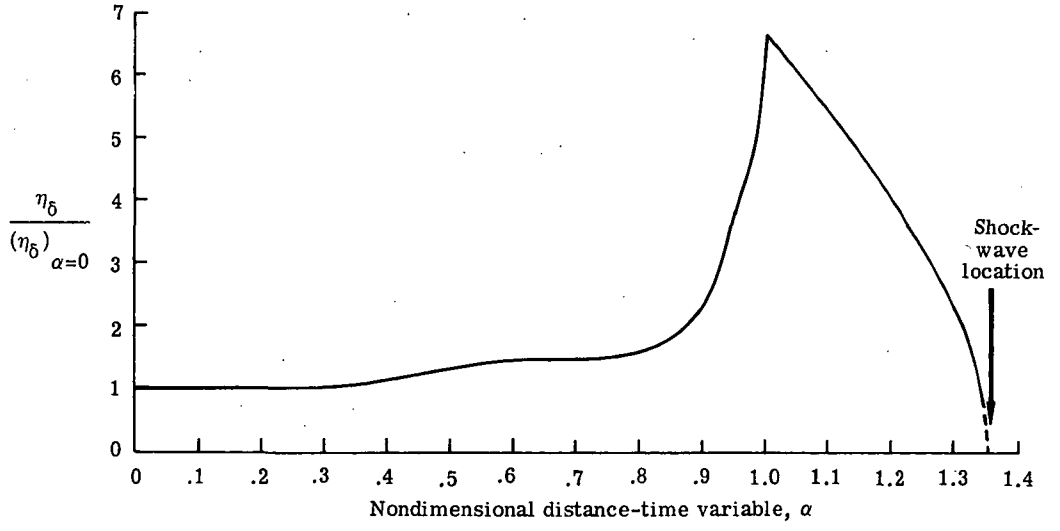

Figure 19.- Relaxation of boundary-layer thickness to Blasuis value $(\eta_\delta)_{\alpha=0}$ for $M_S = 8$ in helium with nitrogen as the test gas. MR limit.

curve may be noted for $\alpha \to 1$. This result is due to the temperature jump contained in the thermal boundary condition at the singular point $\alpha = \beta = 1.0$. As expected, the boundary-layer thickness approaches zero (and the shear function approaches infinity) at the foot of the shock which in this case is at $\alpha = A = 1.356$.

CONCLUDING REMARKS

A theoretical investigation of the relaxation of accelerating gas to the test gas in the boundary layer over a flat plate mounted in an expansion tube has been conducted. The time-dependent compressible laminar boundary-layer equations of a perfect binary gas mixture have been taken as the flow-governing equations. Complete mass and thermal diffusion effects for the binary mixture in the boundary layer have been considered. Self-similar solutions of the governing equations expressed in Crocco variables have been obtained by the Gauss-Seidel line-relaxation method. The results obtained correspond to two limiting cases in which the flow external to the boundary layer on a flat plate can be considered to be similar in time or "conical." These conically similar limits are (1) when the time lag between the arrival of the shock and the interface at the leading edge of the plate is very large; and (2) when this time lag is vanishingly small.

The following assumptions have been made in the present analysis: gases have been treated as the binary mixture of perfect gases, the real-gas viscosity has been used for nitrogen, and the interface has been assumed to be of zero thickness. This last assumption is justified for a thin interface, that is, for the flow situations where the thickness of the interface is small compared with the length of the plate. Also, the relaxation of the boundary layer on the plate surface in the region where the Blasius state exists is not substantially affected by this restriction of zero-thickness interface because the approach to the Blasius value is asymptotic.

The fluid properties required in the numerical evaluation of the equations have been obtained in detail from the exponential potential function, which is considered to be more accurate than the Lennard-Jones potential at high temperatures. A comparison between the properties calculated from these two potential functions at high temperatures is presented.

The numerical results obtained are for shock Mach numbers ranging from 3 to 10 in helium (considered as the accelerating gas). The gas considered in the test section is nitrogen. Argon and nitrogen are also considered as the accelerating gases for shock Mach numbers giving equivalent velocities in the free stream behind the shock. The results obtained predict the time required for an all-helium or an all-argon boundary layer to relax to an all-nitrogen boundary layer at any point on the plate. The results indicate that a steady-state boundary layer containing more than 95-percent test gas ("perfect"

nitrogen) exists over a plate length equal to about three-tenths of the distance traveled by the interface in the free stream from the leading edge. The Stanton number and the local skin-friction coefficient, however, relax to within about 10 percent of the steady-state test-gas value for about four-tenths of the plate surface.

Using a lighter gas (such as helium) as the accelerating gas increases the test time for the case when the shock wave and the interface arrive on the model almost together. However, using a heavier gas (such as argon or nitrogen) as the accelerating gas increases the test time for the case when the interface lags behind the shock wave substantially.

Finally, since the conversion of the boundary layer is near completion for about three-tenths of the plate length in the two limiting situations analyzed here, it is thought that all intermediate cases should lie within the range of the results presented in this report.

Langley Research Center,
National Aeronautics and Space Administration,
Hampton, Va., November 4, 1972.

APPENDIX A

TRANSFORMATION OF FLOW-GOVERNING EQUATIONS

The Crocco dependent variables are

$$\left.\begin{aligned} c &= c(\bar{x},\bar{u},\bar{t}) \\ \tau &= \mu \frac{\partial u}{\partial y} = \tau(\bar{x},\bar{u},\bar{t}) \\ h &= h(\bar{x},\bar{u},\bar{t}) \end{aligned}\right\} \tag{A1}$$

and the independent variables are

$$\left.\begin{aligned} \bar{x} &\equiv x \\ \bar{u} &\equiv u(x,y,t) \\ \bar{t} &\equiv t \end{aligned}\right\} \tag{A2}$$

For a function $F(x,y,t)$ transformed to $F(\bar{x},\bar{u},\bar{t})$, the transformation equations for its derivatives will be

$$\frac{\partial F}{\partial x} = \frac{\partial F}{\partial \bar{x}} + \frac{\partial F}{\partial \bar{u}} \frac{\partial \bar{u}}{\partial x} \tag{A3}$$

$$\frac{\partial F}{\partial y} = \frac{\partial F}{\partial \bar{u}} \frac{\partial \bar{u}}{\partial y} \tag{A4}$$

$$\frac{\partial F}{\partial t} = \frac{\partial F}{\partial \bar{u}} \frac{\partial \bar{u}}{\partial t} + \frac{\partial F}{\partial \bar{t}} \tag{A5}$$

If $F = y$, then

$$\left.\begin{aligned} \frac{\partial y}{\partial x} &= 0 \\ \frac{\partial y}{\partial y} &= 1 \\ \frac{\partial y}{\partial t} &= 0 \end{aligned}\right\} \tag{A6}$$

From equations (A3) and (A6), it follows that

$$\frac{\partial y}{\partial x} = 0 = \frac{\partial y}{\partial \bar{x}} + \frac{\partial y}{\partial \bar{u}} \frac{\partial \bar{u}}{\partial x}$$

or

$$\frac{\partial \bar{u}}{\partial x} = - \frac{\partial y / \partial \bar{x}}{\partial y / \partial \bar{u}} = - \frac{y_{\bar{x}}}{y_{\bar{u}}} \tag{A7}$$

Similarly, from equations (A5) and (A6)

$$\frac{\partial y}{\partial t} = 0 = \frac{\partial y}{\partial \bar{u}} \frac{\partial \bar{u}}{\partial t} + \frac{\partial y}{\partial \bar{t}}$$

or

$$\frac{\partial \bar{u}}{\partial t} = - \frac{y_{\bar{t}}}{y_{\bar{u}}} \tag{A8}$$

Also, from equations (A4) and (A6)

$$\frac{\partial y}{\partial y} = 1 = \frac{\partial y}{\partial \bar{u}} \frac{\partial \bar{u}}{\partial y}$$

or

$$\frac{\partial \bar{u}}{\partial y} = \frac{1}{\partial y / \partial \bar{u}} = \frac{\tau}{\mu} \tag{A9}$$

By using equations (A7), (A8), and (A9) in equations (A3), (A4), and (A5),

$$\frac{\partial F}{\partial x} = \frac{\partial F}{\partial \bar{x}} - \frac{y_{\bar{x}}}{y_{\bar{u}}} \frac{\partial F}{\partial \bar{u}} \tag{A10}$$

$$\frac{\partial F}{\partial y} = \frac{\tau}{\mu} \frac{\partial F}{\partial \bar{u}} \tag{A11}$$

$$\frac{\partial F}{\partial t} = \frac{\partial F}{\partial \bar{t}} - \frac{y_{\bar{t}}}{y_{\bar{u}}} \frac{\partial F}{\partial \bar{u}} \tag{A12}$$

In terms of Crocco's variables, equations (2), (3), and (4) may now be written as

$$\mu \rho \left(\frac{\partial c}{\partial \bar{t}} + \bar{u} \frac{\partial c}{\partial \bar{x}} \right) = \tau^2 \left(\frac{\partial}{\partial \bar{u}} \frac{N_{Le}}{N_{Pr}} \frac{\partial c}{\partial \bar{u}} + \frac{D_1^T}{T} \frac{1}{\mu} \frac{\partial T}{\partial \bar{u}} \right)$$

$$+ \frac{1}{2} \left[\frac{\partial}{\partial \bar{u}} \left(\tau^2 \right) \right] \left[\left(\frac{N_{Le}}{N_{Pr}} - 1 \right) \frac{\partial c}{\partial \bar{u}} + \frac{D_1^T}{T} \frac{1}{\mu} \frac{\partial T}{\partial \bar{u}} \right] \tag{A13}$$

$$\frac{\partial^2 \tau}{\partial \bar{u}^2} + \frac{\partial}{\partial \bar{t}} \left(\frac{\mu \rho}{\tau} \right) + \bar{u} \frac{\partial}{\partial \bar{x}} \left(\frac{\mu \rho}{\tau} \right) = 0 \tag{A14}$$

$$\mu\rho\left(\frac{\partial h}{\partial \bar{t}} + \bar{u}\frac{\partial h}{\partial \bar{x}}\right) = \tau^2\left\{1 + \frac{\partial}{\partial \bar{u}}\left[\frac{1}{N_{Pr}}\frac{\partial h}{\partial \bar{u}} + \frac{N_{Le} - 1}{N_{Pr}}\frac{\partial c}{\partial \bar{u}}h_1(1 - \Gamma) + \frac{D_1{}^T}{T}\frac{1}{\mu}\frac{\partial T}{\partial \bar{u}}\right.\right.$$

$$\left.\left.\times h_1(1 - \Gamma)\right]\right\} + \frac{1}{2}\left[\frac{\partial}{\partial \bar{u}}\left(\tau^2\right)\right]\left[\left(\frac{1}{N_{Pr}} - 1\right)\frac{\partial h}{\partial \bar{u}} + h_1(1 - \Gamma)\right.$$

$$\left.\times\left(\frac{N_{Le} - 1}{N_{Pr}}\frac{\partial c}{\partial \bar{u}} + \frac{D_1{}^T}{T}\frac{1}{\mu}\frac{\partial T}{\partial \bar{u}}\right)\right] \qquad \text{(A15)}$$

In obtaining equations (A13), (A14), and (A15), the overall continuity equation (1) has been utilized.

Next, these equations are transformed to the conical coordinate system. In this system the dimensionless independent variables are

$$\left.\begin{aligned} \alpha &= \frac{\bar{x}}{U_o\bar{t}} \\ \beta &= \frac{\bar{u}}{U_o} \\ \bar{\gamma} &= \frac{\rho_w U_o{}^2\bar{t}}{\mu_w} \end{aligned}\right\} \qquad \text{(A16)}$$

This transformation, although completely general, is subsequently applied to a restricted class of flows in which the free-stream quantities are functions of α alone in order to reduce the complexity of the equations while still retaining all the features necessary for applications to shock-generated flows.

The transformation equations for the derivatives are

$$\left.\begin{aligned} \frac{\partial F}{\partial \bar{x}} &= \frac{1}{U_o\bar{t}}\frac{\partial F}{\partial \alpha} \\ \frac{\partial F}{\partial \bar{u}} &= \frac{1}{U_o}\frac{\partial F}{\partial \beta} \\ \frac{\partial F}{\partial \bar{t}} &= -\frac{\alpha}{\bar{t}}\frac{\partial F}{\partial \alpha} + \frac{U_o{}^2}{\nu_w}\frac{\partial F}{\partial \bar{\gamma}} \end{aligned}\right\} \qquad \text{(A17)}$$

Equations (A13), (A14), and (A15) may now be written, by using equations (A17), as

$$\frac{\tau^2}{U_o{}^2}\frac{\partial}{\partial\beta}\left(\frac{N_{Le}}{N_{Pr}}\frac{\partial c}{\partial\beta}+J\right)+\frac{1}{2U_o{}^2}\left[\frac{\partial}{\partial\beta}\left(\tau^2\right)\right]\left[\left(\frac{N_{Le}}{N_{Pr}}-1\right)\frac{\partial c}{\partial\beta}+J\right]$$

$$=\mu\rho\left(\frac{U_o{}^2}{\nu_w}\frac{\partial c}{\partial\bar{\gamma}}-\frac{\alpha-\beta}{\bar{t}}\frac{\partial c}{\partial\alpha}\right) \tag{A18}$$

$$\frac{\tau^2}{U_o{}^2}\frac{\partial^2\tau}{\partial\beta^2}+\mu\rho\left(\frac{\alpha-\beta}{\bar{t}}\frac{\partial\tau}{\partial\alpha}-\frac{U_o{}^2}{\nu_w}\frac{\partial\tau}{\partial\bar{\gamma}}\right)=\tau\left[\frac{\alpha-\beta}{\bar{t}}\frac{\partial}{\partial\alpha}(\mu\rho)-\frac{U_o{}^2}{\nu_w}\frac{\partial}{\partial\bar{\gamma}}(\mu\rho)\right] \tag{A19}$$

$$\frac{\tau^2}{U_o{}^2}\left\{U_o{}^2+\frac{\partial}{\partial\beta}\left[\frac{1}{N_{Pr}}\frac{\partial h}{\partial\beta}+\frac{N_{Le}-1}{N_{Pr}}\frac{\partial c}{\partial\beta}h_1(1-\Gamma)+Jh_1(1-\Gamma)\right]\right\}+\frac{1}{2U_o{}^2}\left[\frac{\partial}{\partial\beta}\left(\tau^2\right)\right]$$

$$\times\left[\left(\frac{1}{N_{Pr}}-1\right)\frac{\partial h}{\partial\beta}+h_1(1-\Gamma)\left(\frac{N_{Le}-1}{N_{Pr}}\frac{\partial c}{\partial\beta}+J\right)\right]=\mu\rho\left(\frac{U_o{}^2}{\nu_w}\frac{\partial h}{\partial\bar{\gamma}}-\frac{\alpha-\beta}{\bar{t}}\frac{\partial h}{\partial\alpha}\right) \tag{A20}$$

The following dimensionless dependent variables are now introduced:

$$\left.\begin{aligned}
c(\alpha,\beta,\bar{\gamma}) &= c\\
\bar{\phi}(\alpha,\beta,\bar{\gamma}) &= \frac{\tau}{\rho_w U_o{}^2}\\
H(\alpha,\beta,\bar{\gamma}) &= \frac{h-h_w}{h_w}\\
H_1(\alpha,\beta,\bar{\gamma}) &= \frac{h_1-h_w}{h_w}
\end{aligned}\right\} \tag{A21}$$

With the introduction of equations (A21), equations (A18) to (A20) become

$$\bar{\phi}^2\frac{\partial}{\partial\beta}\left(\frac{N_{Le}}{N_{Pr}}\frac{\partial c}{\partial\beta}+J\right)+\bar{\phi}\frac{\partial\bar{\phi}}{\partial\beta}\left[\left(\frac{N_{Le}}{N_{Pr}}-1\right)\frac{\partial c}{\partial\beta}+J\right]=C\left(\frac{\partial c}{\partial\bar{\gamma}}-\frac{\alpha-\beta}{\bar{\gamma}}\frac{\partial c}{\partial\alpha}\right) \tag{A22}$$

$$\bar{\phi}^2\frac{\partial^2\bar{\phi}}{\partial\beta^2}+C\left(\frac{\alpha-\beta}{\bar{\gamma}}\frac{\partial\bar{\phi}}{\partial\alpha}-\frac{\partial\bar{\phi}}{\partial\bar{\gamma}}\right)=\bar{\phi}\left(\frac{\alpha-\beta}{\bar{\gamma}}\frac{\partial C}{\partial\alpha}-\frac{\partial C}{\partial\bar{\gamma}}\right) \tag{A23}$$

$$\overline{\phi}^2\left\{\frac{U_o^2}{h_w}+\frac{\partial}{\partial\beta}\left[\frac{1}{N_{Pr}}\frac{\partial H}{\partial\beta}+\frac{N_{Le}-1}{N_{Pr}}(H_1+1)(1-\Gamma)\frac{\partial c}{\partial\beta}+J(H_1+1)(1-\Gamma)\right]\right\}$$

$$+\overline{\phi}\frac{\partial\overline{\phi}}{\partial\beta}\left[\left(\frac{1}{N_{Pr}}-1\right)\frac{\partial H}{\partial\beta}+(H_1+1)(1-\Gamma)\left(\frac{N_{Le}-1}{N_{Pr}}\frac{\partial c}{\partial\beta}+J\right)\right]=C\left(\frac{\partial H}{\partial\overline{\gamma}}-\frac{\alpha-\beta}{\overline{\gamma}}\frac{\partial H}{\partial\alpha}\right) \tag{A24}$$

The following form for $\overline{\phi}$ is introduced so that the momentum equation (A23) becomes independent of $\overline{\gamma}$:

$$\overline{\phi}(\alpha,\beta,\overline{\gamma})=\frac{\phi(\alpha,\beta)}{\sqrt{\alpha\overline{\gamma}}}=\frac{\phi(\alpha,\beta)}{\sqrt{R_{w,x}}} \tag{A25}$$

For energy equation (A24), the following relationship is assumed:

$$H(\alpha,\beta,\overline{\gamma})=R(\overline{\gamma})\,N(\alpha,\beta)$$

Now $R(\overline{\gamma})$ is specified so that the $\lim_{\overline{\gamma}\to 0} H$ is bounded and equation (A24) is independent of $\overline{\gamma}$. Such a requirement for $R(\overline{\gamma})$ means that $R(\overline{\gamma})$ = Constant and without any loss of generality this constant may be taken as unity.

Hence, $\partial H/\partial\overline{\gamma}=0$ and implies that

$$H=H(\alpha,\beta) \tag{A26}$$

Equation (A26) is the result given by Lam (ref. 4). (It may also be noted from eq. (A25) that $\lim_{\overline{\gamma}\to 0}\phi=0$.) By following an argument similar to that for H, it is found that

$$\left.\begin{aligned} c&=c(\alpha,\beta)\\ \frac{\partial c}{\partial\overline{\gamma}}&=0\end{aligned}\right\} \tag{A27}$$

Also, since $C=C(c,H)$,

$$\frac{\partial C}{\partial\overline{\gamma}}=0 \tag{A28}$$

By utilizing expressions (A25) to (A28) in equations (A22) to (A24), the following form of the governing equations is obtained:

$$\phi^2\frac{\partial}{\partial\beta}\left(\frac{N_{Le}}{N_{Pr}}\frac{\partial c}{\partial\beta}+J\right)+\phi\frac{\partial\phi}{\partial\beta}\left[\left(\frac{N_{Le}}{N_{Pr}}-1\right)\frac{\partial c}{\partial\beta}+J\right]=C\alpha(\beta-\alpha)\frac{\partial c}{\partial\alpha} \tag{A29}$$

$$\phi^2\frac{\partial^2\phi}{\partial\beta^2}+\frac{C\beta}{2}\phi=\alpha(\beta-\alpha)\left(C\frac{\partial\phi}{\partial\alpha}-\phi\frac{\partial C}{\partial\alpha}\right) \tag{A30}$$

$$\phi^2\left\{\frac{U_o^2}{h_w}+\frac{\partial}{\partial\beta}\left[\frac{1}{N_{Pr}}\frac{\partial H}{\partial\beta}+\frac{N_{Le}-1}{N_{Pr}}\left(H_1+1\right)\left(1-\Gamma\right)\frac{\partial c}{\partial\beta}+J\left(H_1+1\right)\left(1-\Gamma\right)\right]\right\}$$

$$+\phi\frac{\partial\phi}{\partial\beta}\left[\left(\frac{1}{N_{Pr}}-1\right)\frac{\partial H}{\partial\beta}+\left(H_1+1\right)\left(1-\Gamma\right)\left(\frac{N_{Le}-1}{N_{Pr}}\frac{\partial c}{\partial\beta}+J\right)\right]=C(\beta-\alpha)\alpha\frac{\partial H}{\partial\alpha} \qquad \text{(A31)}$$

APPENDIX B

SHOCK PARAMETERS IN AN IDEAL GAS

To be consistent with the rest of the analysis and for the sake of simplicity, the following properties of the gas are assumed:

(1) It obeys the ideal equation of state.

(2) $\gamma = c_p/c_v$ = Constant, c_p = Constant.

With these assumptions, the following relations are obtained from reference 25:

$$A = \frac{U_s}{U_o} = \frac{\gamma + 1}{2} \frac{M_s^2}{M_s^2 - 1} \tag{B1}$$

$$\frac{U_o^2}{h_o} = \frac{4(\gamma - 1)}{(\gamma + 1)^2} \frac{T_1}{T_o} \left(M_s - \frac{1}{M_s} \right)^2 \tag{B2}$$

$$\frac{T_o}{T_1} = 1 + \frac{2(\gamma - 1)}{(\gamma + 1)^2} \left[\gamma M_s^2 - \frac{1}{M_s^2} + (1 - \gamma) \right] \tag{B3}$$

where T_1 is the temperature of gas in front of the shock. The temperature T_1 has been taken as T_w (=300 K) in this analysis.

Further,

$$\frac{U_o^2}{h_w} = \frac{U_o^2}{h_o} \frac{h_o}{h_w} = \frac{U_o^2}{h_o} \frac{T_o}{T_1} \tag{B4}$$

since c_p is assumed to be constant and $T_1 = T_w$.

APPENDIX C

THERMODYNAMIC AND TRANSPORT PROPERTIES OF N_2-He AND N_2-Ar MIXTURES

Thermodynamic Properties

N_2-He mixture.- In evaluating the density ρ of the binary mixture, the individual species comprising the gas mixture are assumed to be calorically perfect; that is, the specific heats of the pure species are constant. The density of the mixture of perfect gases is obtained from equation (7):

$$\rho = \frac{p}{T \sum_{i=1,2} c_i R_i}$$

or

$$\rho = \frac{p}{R_1 T} \frac{1}{c + (1 - c)\frac{\overline{M}_1}{\overline{M}_2}} \tag{C1}$$

where R_1 is the gas constant for nitrogen and $\overline{M}_1/\overline{M}_2 = 7$ for the N_2-He binary mixture.

The specific heats for the mixture are given by

$$c_v = cc_{v,1} + (1 - c)c_{v,2} \tag{C2}$$

$$c_p = cc_{p,1} + (1 - c)c_{p,2} \tag{C3}$$

For calorically perfect He and N_2, the following relation is also employed:

$$\frac{c_{p,1}}{c_{p,2}} = \frac{\frac{7}{2}R_1}{\frac{5}{2}R_2} = \frac{1.4}{\overline{M}_1/\overline{M}_2} = 0.2 \tag{C4}$$

Values of $c_{p,2}$, $c_{v,2}$, and R_2 for helium are

$$\left.\begin{aligned} c_{p,2} &= 5.1988 \times 10^3 \frac{m^2}{sec^2\text{-}K} \\ c_{v,2} &= 3.1189 \times 10^3 \frac{m^2}{sec^2\text{-}K} \\ R_2 &= 2.0799 \times 10^3 \frac{m^2}{sec^2\text{-}K} \end{aligned}\right\} \tag{C5}$$

N_2-Ar mixture.- Equations (C1) to (C3) may also be used for obtaining ρ, c_p, and c_v for the N_2-Ar mixture. However, c will represent the mass fraction of Ar, and R_1 will be the gas constant for argon. Other quantities of interest for this case will be

$$\left.\begin{aligned} &\frac{\overline{M}_1}{\overline{M}_2} = 1.429 \\ &\frac{c_{p,1}}{c_{p,2}} = \frac{\frac{5}{2}R_1}{\frac{7}{2}R_2} = \frac{\frac{5}{2}\frac{R'}{40}}{\frac{7}{2}\frac{R'}{28}} = 0.5 \\ &c_{p,1} = 5.2032 \times 10^2 \ \frac{m^2}{sec^2\text{-}K} \\ &c_{v,1} = 3.1171 \times 10^2 \ \frac{m^2}{sec^2\text{-}K} \\ &R_1 = 2.0819 \times 10^2 \ \frac{m^2}{sec^2\text{-}K} \end{aligned}\right\} \tag{C6}$$

Here, R' is the universal gas constant.

Transport Properties

The viscosity of the mixture is given by Wilke's approximate formula (ref. 31) applied to a binary system

$$\mu = \frac{\mu_1}{1 + G_{12}\frac{x_2}{x_1}} + \frac{\mu_2}{1 + G_{21}\frac{x_1}{x_2}} \tag{C7}$$

where μ_1 and μ_2 are the viscosities of the individual species forming the binary mixture and

$$G_{ij} = \frac{\left[1 + \left(\frac{\mu_i}{\mu_j}\right)^{1/2}\left(\frac{\overline{M}_j}{\overline{M}_i}\right)^{1/4}\right]^2}{2\sqrt{2}\left(1 + \frac{\overline{M}_i}{\overline{M}_j}\right)^{1/2}} \qquad (i, j = 1, 2) \tag{C8}$$

$$\left.\begin{aligned} x_1 &= \frac{c}{c + (1 - c)\dfrac{\overline{M}_1}{\overline{M}_2}} \\ x_2 &= \frac{1 - c}{\dfrac{c}{\overline{M}_1/\overline{M}_2} + (1 - c)} \end{aligned}\right\} \tag{C9}$$

N_2-He mixture.- The viscosities of N_2 and He were obtained as follows:

For $300\ K \leqq T \leqq 2000\ K$ (based on ref. 32):

$$\mu_{N_2} = 5.7925 \times 10^{-7} T^{0.613}\ \frac{N\text{-sec}}{m^2} \tag{C10a}$$

For $300\ K \leqq T \leqq 1300\ K$ (based on ref. 33):

$$\mu_{He} = 5.0236 \times 10^{-7} T^{0.647}\ \frac{N\text{-sec}}{m^2} \tag{C10b}$$

For $2000\ K \leqq T \leqq 10\ 000\ K$ (based on ref. 34):

$$\mu_{N_2} = 1.2802 \times 10^{-7} T^{0.811}\ \frac{N\text{-sec}}{m^2} \tag{C11a}$$

For $1300\ K \leqq T \leqq 10\ 000\ K$ (based on ref. 34):

$$\mu_{He} = 1.2858 \times 10^{-7} T^{0.839}\ \frac{N\text{-sec}}{m^2} \tag{C11b}$$

To simplify the present analysis, a mean viscosity-temperature relationship was applied to both gases. This relationship was obtained with the help of equations (C10) and (C11) and references 32 to 34 as shown in figure 20. The mean viscosity formula obtained is

$$\left.\begin{aligned} \mu_{mean} &= 5.4085 \times 10^{-7} T^{0.63}\ \frac{N\text{-sec}}{m^2} && (300\ K \leqq T \leqq 1550\ K) \\ \mu_{mean} &= 1.2908 \times 10^{-7} T^{0.825}\ \frac{N\text{-sec}}{m^2} && (1550\ K \leqq T \leqq 10\ 000\ K) \end{aligned}\right\} \tag{C12}$$

The viscosity obtained from equations (C12) has been fitted to polynomials in temperature by using the method of least squares

$$\mu_{mean} = A + BT + CT^2 + DT^3 + ET^4 + FT^5\ \frac{N\text{-sec}}{m^2} \qquad (300\ K \leqq T \leqq 10\ 000\ K) \tag{C13a}$$

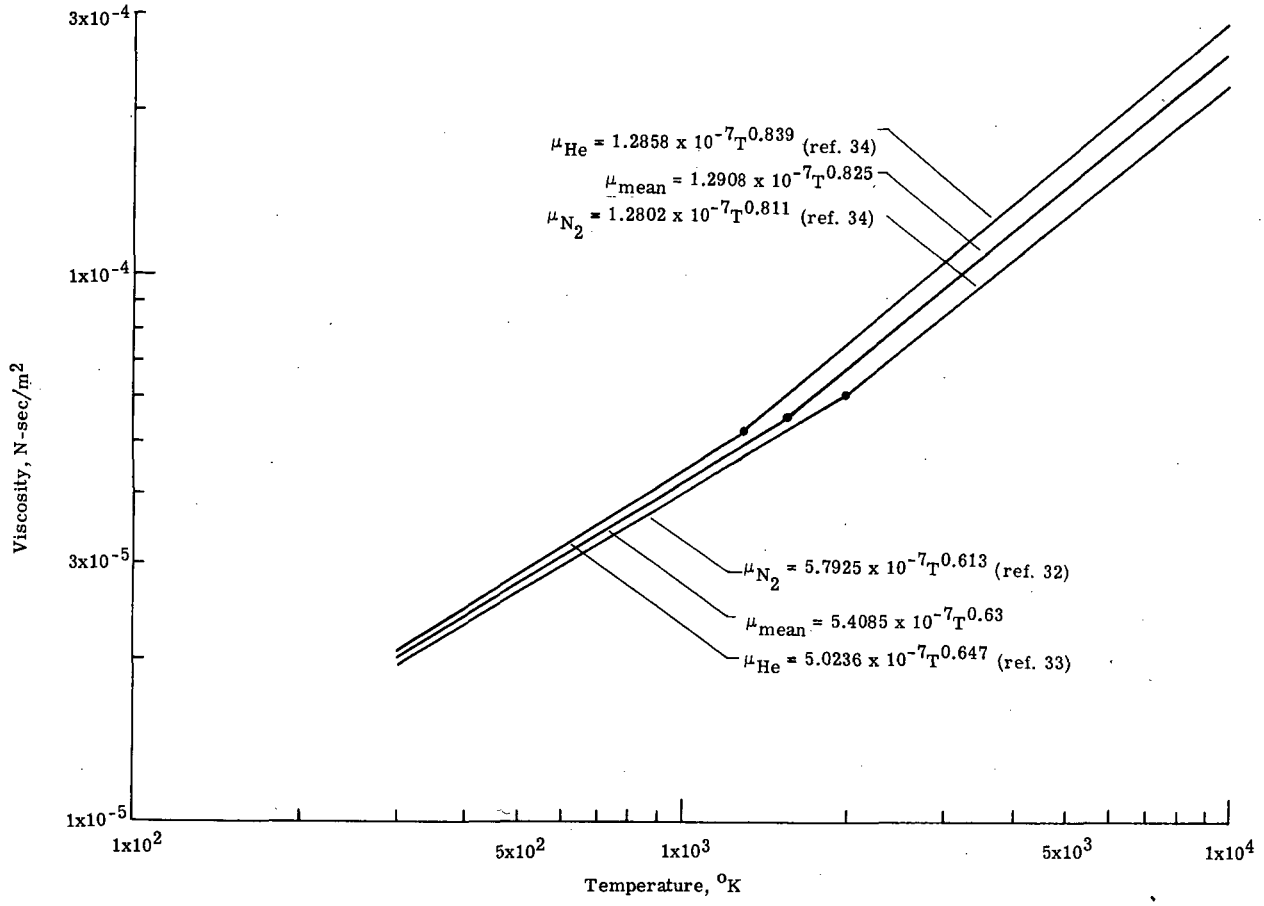

Figure 20.- Temperature variation of helium and nitrogen viscosities and mean value used.

where

$$\left.\begin{aligned} A &= 1.29908164 \times 10^{-5} \\ B &= 2.83599596 \times 10^{-8} \\ C &= -1.63078339 \times 10^{-13} \\ D &= -7.03066415 \times 10^{-17} \\ E &= 6.29878349 \times 10^{-21} \\ F &= -1.53160089 \times 10^{-25} \end{aligned}\right\} \qquad \text{(C13b)}$$

This fitting has been done to remove the discontinuity in the slope of the viscosity curve at 1550 K. The μ_{mean} obtained from these polynomials is displayed in figure 21.

For temperatures higher than 10 000 K, the viscosity of N_2 may be obtained from the work of Yos (ref. 29). These data have been fitted to polynomials in temperature:

$$\mu_{N_2} = A + BT + CT^2 + DT^3 + ET^4 + FT^5 + GT^6 \ \frac{N\text{-sec}}{m^2} \qquad \text{(C14a)}$$

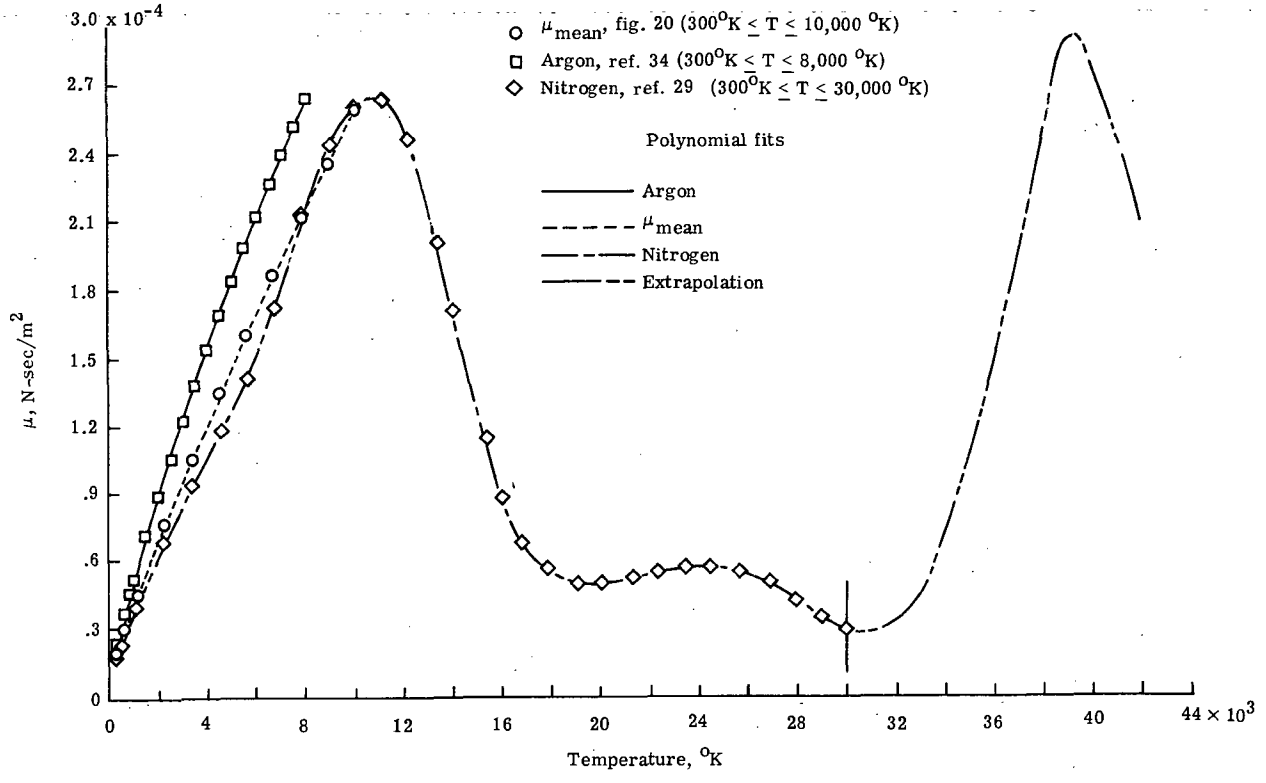

Figure 21.- Polynomial fits in temperature to various viscosities.

where

For 300 K ≦ T ≦ 10 000 K:

$$\left.\begin{aligned} A &= 3.01575924 \times 10^{-5} \\ B &= -1.3942708 \times 10^{-8} \\ C &= 2.94077531 \times 10^{-11} \\ D &= -1.00839516 \times 10^{-14} \\ E &= 1.6046776 \times 10^{-18} \\ F &= -1.15742765 \times 10^{-22} \\ G &= 3.03739295 \times 10^{-27} \end{aligned}\right\} \quad \text{(C14b)}$$

For 10 000 K ≦ T ≦ 20 000 K:

$$\left.\begin{aligned} A &= 4.28597628 \times 10^{-2} \\ B &= -1.85480431 \times 10^{-5} \\ C &= 3.27841650 \times 10^{-9} \\ D &= -3.00995582 \times 10^{-13} \\ E &= 1.51565354 \times 10^{-17} \\ F &= -3.98056198 \times 10^{-22} \\ G &= 4.27318273 \times 10^{-27} \end{aligned}\right\} \quad \text{(C14c)}$$

For 20 000 K ≦ T ≦ 30 000 K:

$$\left.\begin{aligned} A &= -3.23611473 \times 10^{-2} \\ B &= 7.97818283 \times 10^{-6} \\ C &= -8.06518064 \times 10^{-10} \\ D &= 4.27745175 \times 10^{-14} \\ E &= -1.25286254 \times 10^{-18} \\ F &= 1.91811505 \times 10^{-23} \\ G &= -1.19731314 \times 10^{-28} \end{aligned}\right\} \qquad \text{(C14d)}$$

Figure 21 shows the curve for viscosity obtained from these polynomials. This figure also contains the extrapolation of this polynomial fit to 42 000 K. This extrapolation was used in the evaluation of boundary-layer parameters for shock Mach number of 26.1 in nitrogen, since no viscosity data exist for nitrogen for temperatures higher than 30 000 K.

The thermal conductivities of the individual species are given by the Eucken relation (ref. 22, p. 499)

$$k_i = \frac{1}{4}\left(\frac{c_{p,i}}{c_{v,i}} - 5\right)c_{v,i}\mu_i \qquad (i = N_2, He) \qquad \text{(C15)}$$

The mixture conductivity, as shown in reference 35, is obtained by replacing the viscosities of the species, μ_1 and μ_2, in equation (C7) with the conductivities k_1 and k_2 given by equation (C15). The quantities G_{ij} given by equation (C8) are still evaluated by using the pure species viscosities (ref. 35).

The binary diffusion coefficient is computed by the expression (see ref. 22, p. 539)

$$pD_{12} = 0.002628\,\frac{T^{3/2}\left[\left(\overline{M}_1 + \overline{M}_2\right)/2\overline{M}_1\overline{M}_2\right]^{1/2}}{\sigma_{12}^2\,\Omega_{12}^{(1,1)^*}}\,\frac{\text{atm-cm}^2}{\text{sec}} \qquad \text{(C16)}$$

where σ_{12} is some length parameter defined by the potential function ϕ.

The collision integral $\Omega_{12}^{(1,1)^*}$ in expression (C16) depends on the choice of molecular interaction potential. This integral has been evaluated by Monchick (ref. 2) on the basis of the potential

$$\phi = Ae^{-r/\rho} \qquad \text{(C17)}$$

where A and ρ are (ref. 34)

	A, J	ρ, m
He - He	6.18411×10^{-17}	2.20×10^{-11}
N_2 - N_2	2.16284×10^{-15}	2.63×10^{-11}

For the mixtures, the following combination rules (ref. 34) are used:

$$\left.\begin{aligned} A_{12} &= (A_1 A_2)^{1/2} \\ \frac{1}{\rho_{12}} &= \frac{1}{2}\left(\frac{1}{\rho_1} + \frac{1}{\rho_2}\right) \end{aligned}\right\} \tag{C18}$$

The parameters which are most useful in fitting transport properties are ρ and α, where

$$\alpha = \ln \frac{A}{\kappa T} \tag{C19}$$

Here κ is the Boltzmann gas constant and T is the absolute temperature in kelvins. By following Monchick (ref. 2), the integrals of interest to gas transport theory may be put in the form

$$\Omega^{(1,1)} = \left(\frac{\kappa T}{8\pi\mu}\right)^{1/2} \int_0^\infty dx\, x^2 e^{-x} Q^{(1)}(x) \tag{C20}$$

with

$$Q^{(1)}(x) = 2\pi \int_0^\infty \left[1 - \cos \chi(x)\right] b\, db \tag{C21}$$

and

$$x = \frac{\mu g^2}{2\kappa T} \tag{C22}$$

where μ is the reduced mass, g the relative velocity, and b the impact parameter. For a given ϕ (intermolecular potential), χ is given by

$$\chi = \pi - 2 \int_{r_o}^\infty \frac{r^{-2} b\, dr}{\left(1 - \frac{b^2}{r^2} - \frac{2\phi}{\mu g^2}\right)^{1/2}} \tag{C23}$$

Here r_o is the distance of closest approach.

With certain simplifying assumptions (ref. 2), χ may be rewritten as

$$\chi = \pi - 4k' \theta_o \tag{C24}$$

where

$$k' = \int_0^1 \left\{1 - \frac{\cos^2 \theta_o}{\cos^2 \theta} \exp\left[\frac{1 - 4\xi \ln u}{\xi}\left(1 - \frac{\sin \theta_o}{\sin \theta}\right)\right]\right\}^{-1/2} z\, dz \tag{C25}$$

$$\left.\begin{aligned} \theta_o &= \sin^{-1}\frac{b}{r_o} \\ \theta &= \sin^{-1}\frac{b}{r} \end{aligned}\right\} \tag{C26}$$

$$\left.\begin{aligned} \xi &= \frac{1}{\alpha - \ln x} \\ u^2 &= \cos\theta_o \\ z^2 &= 1 - \frac{\theta}{\theta_o} \end{aligned}\right\} \tag{C27}$$

With the help of equation (C24), equation (C21) may be simplified to

$$Q^{(1)} = \frac{8\pi\rho^2}{\xi^2} I_1'(x) \tag{C28}$$

where

$$I_1'(x) = \int_0^1 du(1 - \cos\chi)\left\{\frac{u^3}{2} + \xi\left[\frac{1}{u} - u^3(4\ln u + 1)\right] + \xi^2\left[4\ln u\left(2u^3\ln u + u^3 - \frac{1}{u}\right)\right]\right\} \tag{C29}$$

By utilizing equation (C28), expression (C20) may finally be put in the form

$$\Omega^{(1,1)} = 4\left(\frac{\pi\kappa T}{2\mu}\right)^{1/2}\alpha^2\rho^2 I_{(1,1)} \tag{C30}$$

where

$$I_{(1,1)} = 4\int_0^1 t^3(-4\ln t)^2\left[1 - \frac{\ln(-4\ln t)}{\alpha}\right]^2 I_1'\,dt \tag{C31}$$

and

$$t = e^{-x/4}$$

Monchick (ref. 2) has provided the tabulation of integral $I_{(1,1)}$ as a function of α.

Hirschfelder et al. (ref. 22, p. 526) have given their formulas for transport properties for the first approximation in terms of the quantities

$$\sigma_{12}^2\Omega_{12}^{(1,1)*} = \frac{\left(\frac{2\pi\mu}{\kappa T}\right)^{1/2}\Omega^{(1,1)}}{\frac{\pi}{2}(2)!} \tag{C32}$$

Substituting for $\Omega^{(1,1)}$ from equation (C30), equation (C32) yields

$$\sigma_{12}^2 \Omega_{12}^{(1,1)^*} = \frac{8\alpha^2\rho^2 I_{(1,1)}}{2!} \tag{C33}$$

By using equation (C33) in expression (C16), the following relation is obtained for the binary diffusion coefficient:

$$pD_{12} = \frac{4.3822 \times 10^{-2} T^{3/2}}{\alpha^2 I_{(1,1)}} \text{ N/sec} \tag{C34}$$

where T is the absolute temperature in kelvins. Figure 22 shows the plot of pD_{12} as a function of temperature. Polynomial representation of this function is given as follows:

$$pD_{12} = A + BT + CT^2 + DT^3 + ET^4 + FT^5 \text{ N/sec} \qquad (300 \text{ K} \leqq T \leqq 10\,000 \text{ K}) \tag{C35a}$$

where

$$\left.\begin{aligned} A &= -4.20571429 \times 10^{0} \\ B &= 2.48592499 \times 10^{-2} \\ C &= 4.10466471 \times 10^{-5} \\ D &= -2.16644279 \times 10^{-9} \\ E &= 1.49001648 \times 10^{-13} \\ F &= -4.43803342 \times 10^{-18} \end{aligned}\right\} \tag{C35b}$$

If, instead of using the Monchick's potential to obtain $\Omega_{12}^{(1,1)^*}$ and pD_{12}, the Lennard-Jones (6-12) potential is employed, the coefficients for the polynomial fit (eq. (C35a)) become:

$$\left.\begin{aligned} A &= -5.13254756 \times 10^{0} \\ B &= 2.95342073 \times 10^{-2} \\ C &= 3.14445935 \times 10^{-5} \\ D &= -1.93226973 \times 10^{-9} \\ E &= 1.27828289 \times 10^{-13} \\ F &= -3.92041533 \times 10^{-18} \end{aligned}\right\} \tag{C35c}$$

For Lennard-Jones (6-12) potential, the following force constants are required (ref. 22):

	σ, m	ϵ/κ, K
He - He	2.576×10^{-10}	10.22
N_2 - N_2	3.749×10^{-10}	79.80

where ϵ/κ is the molecular potential energy parameter.

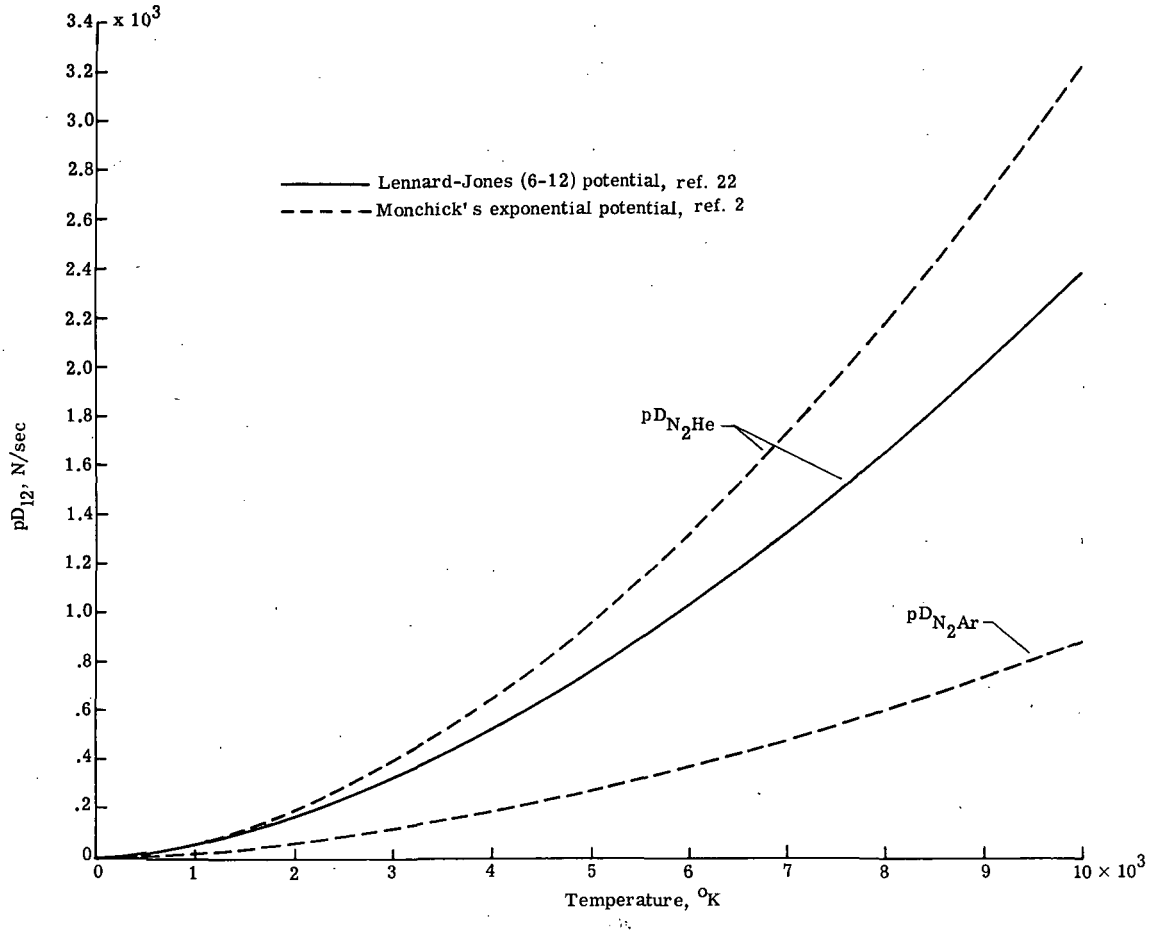

Figure 22.- Product of pressure and binary diffusion coefficient as a function of temperature.

For the binary mixture, the following combination laws (ref. 22) are employed:

$$\left.\begin{aligned} \sigma_{12} &= \frac{\sigma_1 + \sigma_2}{2} \\ \epsilon_{12} &= \sqrt{\epsilon_1 \epsilon_2} \end{aligned}\right\} \qquad \text{(C36)}$$

where the subscript 1 refers to a heavy gas, subscript 2 to a light gas. The integrals $\Omega_{12}^{(1,1)^*}$ for the Lennard-Jones potential are tabulated in reference 22 as functions of reduced temperature $T^* \left(= \kappa T/\epsilon_{12}\right)$. Although these tabulations give $\Omega_{12}^{(1,1)^*}$ for temperatures greater than 10 000 K, pD_{12} obtained from equation (C16) may not be very accurate beyond 1000 K, the reason being that the force constants required in equation (C16) are obtained from viscosity data generally in the range from 300 K to 1000 K. For the sake of comparison the values of pD_{12} obtained from Monchick's exponential potential and Lennard-Jones (6-12) potential have been included in figure 22. The two molecular interaction potentials seem to give the same values for pD_{12} for temperatures

less than 1000 K. For higher temperatures, the two diverge considerably. In the present analysis, Monchick's exponential potential is used and, accordingly, equation (C34) has been employed for the nitrogen-helium mixture.

N_2-Ar mixture.- Viscosity of nitrogen based on Yos work (ref. 29) is given in the preceding section. The viscosity of argon has been obtained from reference 34. A polynomial fit in temperature is

$$\mu_{Ar} = A + BT + CT^2 + DT^3 + ET^4 + FT^5 \frac{N\text{-sec}}{m^2} \tag{C37a}$$

where

$$\left.\begin{aligned} A &= 9.25225746 \times 10^{-6} \\ B &= 4.97493659 \times 10^{-8} \\ C &= -7.76309600 \times 10^{-12} \\ D &= 1.70928912 \times 10^{-15} \\ E &= -1.91727863 \times 10^{-19} \\ F &= 8.02545298 \times 10^{-24} \end{aligned}\right\} \tag{C37b}$$

The viscosity curve is displayed in figure 21.

The viscosity of the N_2-Ar mixture is obtained by using equations (C7) to (C9) along with equations (C14) and (C37) The thermal conductivity of the N_2-Ar mixture may be obtained from equation (C7) with μ_1 and μ_2 replaced by k_1 and k_2 obtained from equation (C15). The expression for the binary diffusion coefficient (using the Monchick exponential potential (ref. 2)) for N_2-Ar mixture is

$$pD_{12} = \frac{1.9816 \times 10^{-2} \times T^{3/2}}{\alpha^2 I_{(1,1)}} \text{ N/sec} \tag{C38}$$

where T is the temperature in kelvins and $I_{(1,1)}$ is tabulated as a function of α by Monchick. Figure 22 also shows a plot of pD_{12} as a function of temperature. Polynomial representation of this function when the collision integral is based on Monchick's exponential function is

$$pD_{12} = A + BT + CT^2 + DT^3 + ET^4 + FT^5 \text{ N/sec} \qquad (300 \text{ K} \leqq T \leqq 10\,000 \text{ K}) \tag{C39a}$$

where

$$\left.\begin{aligned} A &= -1.42368974 \times 10^{0} \\ B &= 8.50226955 \times 10^{-3} \\ C &= 1.17660819 \times 10^{-5} \\ D &= -7.3425527 \times 10^{-10} \\ E &= 5.01785482 \times 10^{-14} \\ F &= -1.49447415 \times 10^{-18} \end{aligned}\right\} \tag{C39b}$$

Transport by Thermal Diffusion

Thermal diffusion transport has been included in the analysis of He-N_2 mixture. The coefficient of thermal diffusion $D_1{}^T$ is obtained from the thermal diffusion factor $(\alpha_T)_1$ through (see ref. 36)

$$D_1{}^T = \rho c(1 - c)D_{12}(\alpha_T)_1 \tag{C40}$$

The thermal diffusion factor for the N_2-He system was computed by using the formula

$$(\alpha_T)_1 = \left(6C_{12}^* - 5\right)\frac{x_1S_1 - x_2S_2}{x_1{}^2Q_1 + x_2{}^2Q_2 + x_1x_2Q_{12}} \tag{C41}$$

given by Amdur and Mason (ref. 34) based upon Kihara's first approximation.

The species mole fraction x_i is related to the species mass fraction c_i and the species molecular weight M_i by equation (C9).

The quantities S_1, Q_1, and Q_{12} are given by

$$S_1 = \frac{5}{3}\frac{\overline{M}_1{}^2}{\overline{M}_1 + \overline{M}_2}\frac{pD_{12}}{\mu_1 R'T} - \frac{4\overline{M}_1\overline{M}_2A_{12}^*}{\left(\overline{M}_1 + \overline{M}_2\right)^2} + \frac{15\overline{M}_2\left(\overline{M}_1 - \overline{M}_2\right)}{2\left(\overline{M}_1 + \overline{M}_2\right)^2} \tag{C42}$$

$$Q_1 = \frac{10}{3}\frac{\overline{M}_1}{\left(\overline{M}_1 + \overline{M}_2\right)^2}\frac{pD_{12}}{\mu_1 R'T}\left(\overline{M}_1{}^2 + 3\overline{M}_2{}^2 + \frac{8}{5}\overline{M}_1\overline{M}_2A_{12}^*\right) \tag{C43}$$

$$Q_{12} = 15\left(\frac{\overline{M}_1 - \overline{M}_2}{\overline{M}_1 + \overline{M}_2}\right)^2 + \frac{32\overline{M}_1\overline{M}_2A_{12}^*}{\left(\overline{M}_1 + \overline{M}_2\right)^2} + \frac{20}{9}\overline{M}_1\overline{M}_2\left(\frac{pD_{12}}{\mu_1 R'T}\right)\left(\frac{pD_{12}}{\mu_2 R'T}\right) \tag{C44}$$

The expressions for S_2 and Q_2 are obtained from those for S_1 and Q_1 by interchanging the subscripts, which refer to the molecular species. Conventionally, the subscript 1 refers to the heavy molecules (N_2) and 2 to the light molecules (He). The quantities μ_1 and μ_2 (which are approximated by μ_{mean} for N_2-He mixture) are given in equations (C13); pD_{12} is given in equations (C35). The quantities C_{12}^* in equation (C41) and A_{12}^* in equation (C42) are dependent on the molecular interaction potential. These quantities have been evaluated by using both Monchick's exponential potential (ref. 2) and Lennard-Jones (6-12) potential (ref. 22). In the analysis C_{12}^* and A_{12}^*, based on Monchick's potential, were used for reasons mentioned earlier in this appendix.

The polynomial representations of C_{12}^* and A_{12}^* are when the collision integral is based on Monchick's exponential function:

$$C_{12}^* = A + BT + CT^2 + DT^3 + ET^4 + FT^5 \qquad (300\ K \leqq T \leqq 10\ 000\ K) \qquad (C45a)$$

where

$$\left.\begin{aligned} A &= 9.4155049 \times 10^{-1} \\ B &= -1.35458159 \times 10^{-5} \\ C &= 3.97227856 \times 10^{-9} \\ D &= -6.93246982 \times 10^{-13} \\ E &= 5.99399177 \times 10^{-17} \\ F &= -1.99707667 \times 10^{-21} \end{aligned}\right\} \qquad (C45b)$$

$$A_{12}^* = A + BT + CT^2 + DT^3 + ET^4 + FT^5 \qquad (300\ K \leqq T \leqq 10\ 000\ K) \qquad (C45c)$$

where

$$\left.\begin{aligned} A &= 1.1481258 \times 10^{0} \\ B &= 2.63688624 \times 10^{-5} \\ C &= -7.96613389 \times 10^{-9} \\ D &= 1.39947611 \times 10^{-12} \\ E &= -1.21357946 \times 10^{-16} \\ F &= 4.04994908 \times 10^{-21} \end{aligned}\right\} \qquad (C45d)$$

and when collision integral is based on Lennard-Jones (6-12) potential:

$$C_{12}^* = A + BT + CT^2 + DT^3 + ET^4 + FT^5 \qquad (300\ K \leqq T \leqq 10\ 000\ K) \qquad (C46a)$$

where

$$\left.\begin{aligned} A &= 9.4356924 \times 10^{-1} \\ B &= 6.59447100 \times 10^{-6} \\ C &= -3.07984512 \times 10^{-9} \\ D &= 6.332799089 \times 10^{-13} \\ E &= -5.91981573 \times 10^{-17} \\ F &= 2.05628180 \times 10^{-21} \end{aligned}\right\} \qquad (C46b)$$

$$A_{12}^* = A + BT + CT^2 + DT^3 + ET^4 + FT^5 \qquad (300\ K \leqq T \leqq 10\ 000\ K) \qquad (C46c)$$

where

$$\left.\begin{aligned} A &= 1.1024645 \times 10^{0} \\ B &= 3.02127930 \times 10^{-5} \\ C &= -1.05877112 \times 10^{-8} \\ D &= 1.93950613 \times 10^{-12} \\ E &= -1.69594890 \times 10^{-16} \\ F &= 5.62715486 \times 10^{-21} \end{aligned}\right\} \qquad (C46d)$$

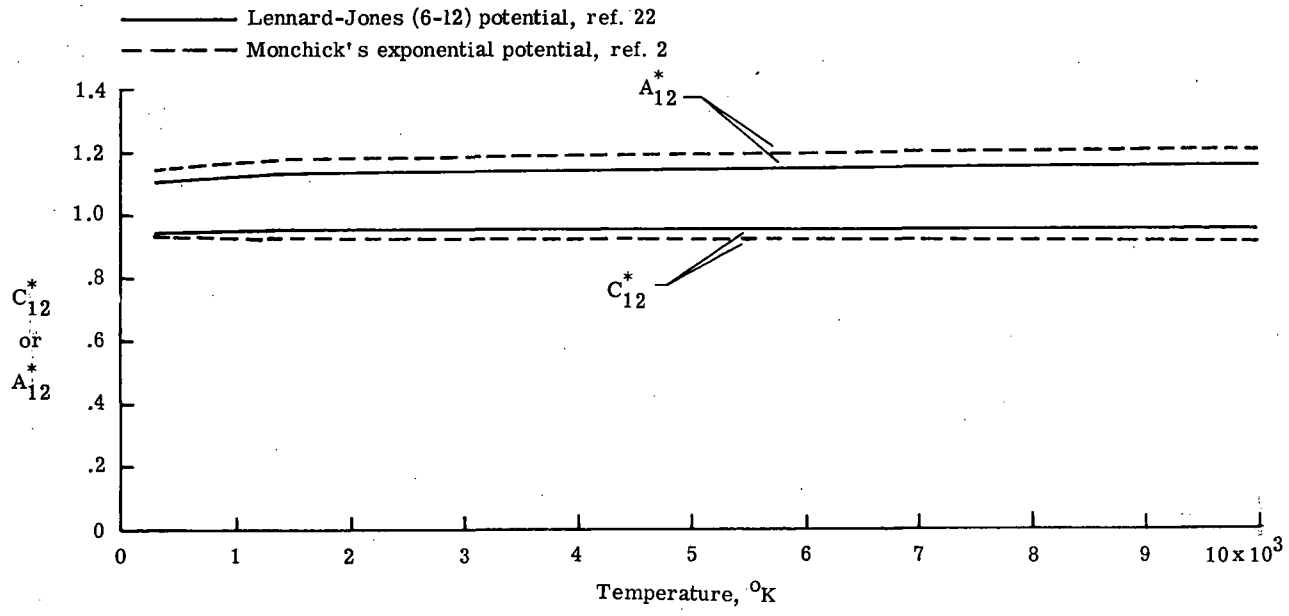

Figure 23.- Molecular thermal diffusion factor parameters as functions of temperature.

These functions are displayed in figure 23.

The fluid properties evaluated in this appendix may now be used to obtain some useful relations required in the solution of the governing equations.

N_2-He mixture.- Employing equations (C1), (C4), (C7), (C8), (C9), and the assumption $\mu_1 \approx \mu_2 \approx \mu_{mean}$, the following relation is obtained for C:

$$C = \frac{\mu\rho}{\mu_w\rho_w}$$

$$= \frac{\mu_{mean}}{\mu_{w,mean}} \frac{1}{H+1} \frac{1 - 0.8c}{1 - 0.8c_w} \frac{1 - 0.857c_w}{1 - 0.857c} \frac{\dfrac{c}{2.282 - 1.282c} + \dfrac{1-c}{1 - 0.674c}}{\dfrac{c_w}{2.282 - 1.282c_w} + \dfrac{1-c_w}{1 - 0.674c_w}} \tag{C47}$$

The value of μ_{mean} required in equation (C47) may be obtained from equations (C13).

Another important quantity required in the analysis is defined by J (the thermal diffusion factor):

$$J = \frac{D_1{}^T}{T} \frac{1}{\mu} \frac{\partial T}{\partial \beta} \tag{C48}$$

Now,

$$\frac{1}{T}\frac{\partial T}{\partial \beta} = \frac{1}{H+1}\frac{\partial H}{\partial \beta} + \frac{0.8}{1-0.8c}\frac{\partial c}{\partial \beta} \tag{C49}$$

By making use of equations (C1), (C7), (C8), (C9), (C40), (C49), and the assumption $\mu_1 \approx \mu_2 \approx \mu_{mean}$, expression (C48) may be written as

$$J = \left[\frac{3.3655 \times 10^{-3}\, c(1-c)(pD_{12})(\alpha_T)_1}{T(7-6c)} \times \frac{1}{\mu_{mean}\left(\frac{c}{2.282-1.282c} + \frac{1-c}{1-0.674c}\right)}\right] \times \left(\frac{1}{H+1}\frac{\partial H}{\partial \beta} - \frac{\frac{c_{p,1}}{c_{p,2}} - 1}{c\frac{c_{p,1}}{c_{p,2}} + 1 - c}\frac{\partial c}{\partial \beta}\right)$$

Or, by using relation (C4),

$$J = \frac{3.3655 \times 10^{-3}}{T\mu_{mean}}\left[\frac{c(1-c)(pD_{12})(\alpha_T)_1}{(7-6c)\left(\frac{c}{2.282-1.282c} + \frac{1-c}{1-0.674c}\right)}\right] \times \left(\frac{1}{H+1}\frac{\partial H}{\partial \beta} + \frac{0.8}{1-0.8c}\frac{\partial c}{\partial \beta}\right) \tag{C50}$$

where μ_{mean} and pD_{12} may be obtained from equations (C13) and (C35). The quantity $(\alpha_T)_1$ may be evaluated from equation (C41) by using relations (C9) and (C42) to (C44) along with equations (C45). For obtaining T, the following relation, based on definitions (A21), may be utilized:

$$T = T_w(H+1)\frac{1-0.8c_w}{1-0.8c} \tag{C51}$$

N_2-Ar mixture.- Expression similar to equation (C47) may also be obtained for the nitrogen-argon mixture by taking into account the appropriate thermodynamic and transport properties. The expression is

$$C = \frac{\mu\rho}{\mu_w \rho_w}$$

$$= \left[\frac{\dfrac{\mu_1 c}{1.188 - 0.188c} + \dfrac{\mu_2(1 - c)}{1 - 0.168c}}{\dfrac{\mu_{w,1} c_w}{1.188 - 0.188c_w} + \dfrac{\mu_{w,2}(1 - c_w)}{1 - 0.168c_w}} \right] \frac{1}{H + 1} \frac{1 - 0.5c}{1 - 0.5c_w} \frac{1.429 - 0.429c_w}{1.429 - 0.429c} \tag{C52}$$

The quantities μ_1 and μ_2, required in expression (C52), may be obtained from equations (C14) and (C37).

Transport due to thermal diffusion was not considered for the N_2-Ar mixture and, therefore, the thermal diffusion factor J was taken as zero in the analysis for this case.

REFERENCES

1. Trimpi, Robert L.: A Preliminary Theoretical Study of the Expansion Tube, a New Device for Producing High-Enthalpy Short-Duration Hypersonic Gas Flows. NASA TR R-133, 1962.

2. Monchick, Louis: Collision Integrals for the Exponential Repulsive Potential. Phys. Fluids, vol. 2, no. 6, Nov.-Dec. 1959, pp. 695-700.

3. Gevrey, M.: Sur les Equations aux Derivees Partielles du Type Parabolique. Journ. de Math., vol. 10, ser. 6, 1914, pp. 105-142.

4. Lam, Sau-Hai: Shock Induced Unsteady Laminar Compressible Boundary Layers on a Semi-Infinite Flat Plate. Ph.D. Thesis, Princeton Univ., 1958.

5. Trimpi, Robert L.; and Cohen, Nathaniel B.: A Theory for Predicting the Flow of Real Gases in Shock Tubes With Experimental Verification. NACA TN 3375, 1955.

6. Trimpi, Robert L.; and Cohen, Nathaniel B.: An Integral Solution to the Flat-Plate Laminar Boundary-Layer Flow Existing Inside and After Expansion Waves and After Shock Waves Moving Into Quiescent Fluid With Particular Application to the Complete Shock-Tube Flow. NACA TN 3944, 1957.

7. Mirels, Harold: Laminar Boundary Layer Behind Shock Advancing Into Stationary Fluid. NACA TN 3401, 1955.

8. Mirels, Harold: Boundary Layer Behind Shock or Thin Expansion Wave Moving Into Stationary Fluid. NACA TN 3712, 1956.

9. Cohen, Nathaniel B.: A Power-Series Solution for the Unsteady Laminar Boundary-Layer Flow in an Expansion Wave of Finite Width Moving Through a Gas Initially at Rest. NACA TN 3943, 1957.

10. Becker, E.: Instationäre Grenzschichten Hinter Verdichlungsstössen und Expansionswellen. Progress in Aeronautical Sciences, Vol. 1, Antonio Ferri, D. Küchemann, and L. H. G. Sterne, eds., Pergamon Press, Inc., 1961, pp. 104-173.

11. Kurzrock, J. W.: Exact Numerical Solutions of the Time-Dependent Compressible Navier-Stokes Equations. CAL Rep. No. AG-2026-W-1, Cornell Aeronaut. Lab., Inc., Feb. 1966.

12. Gupta, Roop N.: The Non-Linear Problem in the Interaction Region of a Shock-Tube Boundary Layer. AIAA J., vol. 11, no. 3, Mar. 1973.

13. Ban, S. D.; and Kuerti, G.: The Interaction Region in the Boundary Layer of a Shock Tube. J. Fluid Mech., vol. 38, 1969, pp. 109-125.

14. Ackroyd, J. A. D.: On the Laminar Compressible Boundary Layer Induced by the Passage of Plane Shock Wave Over a Flat Wall. Proc. Cambridge Phil. Soc., vol. 63, pt. 3, July 1967, pp. 889-907.

15. Stewartson, K.: On the Impulsive Motion of a Flat Plate in a Viscous Fluid. Quart. J. Mech. and Appl. Math., vol. IV, pt. 2, June 1951, pp. 182-198.

16. Lam, S. H.; and Crocco, L.: Note on the Shock-Induced Unsteady Laminar Boundary Layer on a Semi-Infinite Flat Plate. J. Aero/Space Sci., vol. 26, no. 1, 1959, pp. 54-56.

17. Davies, W. R.; and Bernstein, L.: Heat Transfer and Transition to Turbulence in the Shock-Induced Boundary Layer on a Semi-Infinite Flat Plate. J. Fluid Mech., vol. 36, pt. 1, Mar. 1969, pp. 87-112.

18. Felderman, E. J.: Heat Transfer and Shear Stress in the Shock-Induced Unsteady Boundary Layer on a Flat Plate. AIAA J., vol. 6, no. 3, Mar. 1968, pp. 408-412.

19. Ero, Michael Iserhien Osarugiuwa: Shock Induced Unsteady Flow of a Compressible Real Gas Over a Flat Plate. Ph.D. Thesis, Purdue Univ., June 1968.

20. Rodkiewicz, Czeslaw M.; and Reshotko, Eli: Time-Dependent Hypersonic Viscous Interactions. AFOSR 67-2451, U.S. Air Force, Nov. 1967.

21. Gupta, Roop N.; and Rodkiewicz, Czeslaw M.: Unsteady Boundary-Layer Induced Pressures at Hypersonic Speed. Phys. Fluids, vol. 14, no. 7, July 1971, pp. 1332-1339.

22. Hirschfelder, Joseph O.; Curtiss, Charles F.; and Bird, R. Byron: Molecular Theory of Gases and Liquids. John Wiley & Sons, Inc., c.1954. (Reprinted with corrections 1964.)

23. Moore, F. K.: Hypersonic Boundary Layer Theory. Theory of Laminar Flows. Vol. IV of High Speed Aerodynamics and Jet Propulsion, F. K. Moore, ed., Princeton Univ. Press, 1964, pp. 439-527.

24. Clutter, Darwin W.; Smith, A. M. O.; and Jaffe, N. A.: General Method for Solving Nonequilibrium Laminar-Boundary-Layer Flow of a Binary Gas. Rep. No. LB 31616 (Contract NOw-60-0533c), Douglas Aircraft Co., Inc., Oct. 15, 1964.

25. Gaydon, A. G.; and Hurle, I. R.: The Shock Tube in High-Temperature Chemical Physics. Reinhold Pub. Corp., 1963.

26. Ames, William F.: Numerical Methods for Partial Differential Equations. Barnes & Noble, Inc., c.1969.

27. Jaffe, N. A.: The Numerical Solution of the Nonsimilar Laminar Boundary-Layer Equations Including the Effects of Nonequilibrium Dissociation. Paper 5550, Douglas Aircraft Co., Inc., Feb. 1969.

28. Lam, S. H.: Numerical Solutions of Shock-Induced Unsteady Boundary Layers. AFOSR TN 59-926, U.S. Air Force, Aug. 1959.

29. Yos, Jerrold M.: Transport Properties of Nitrogen, Hydrogen, Oxygen, and Air to 30,000° K. RAD-TM-63-7 (Contract AF 33(616)-7578), AVCO Corp., Mar. 22, 1963.

30. Trimpi, Robert L.: A Theoretical Investigation of Simulation in Expansion Tubes and Tunnels. NASA TR R-243, 1966.

31. Wilke, C. R.: A Viscosity Equation for Gas Mixtures. J. Chem. Phys., vol. 18, no. 4, Apr. 1950, pp. 517-519.

32. Hilsenrath, Joseph; Beckett, Charles W.; et al.: Tables of Thermal Properties of Gases. NBS Circ. 564, U.S. Dep. Com., 1955.

33. Keesom, W. H.: Helium. Elsevier, 1942.

34. Amdur, I.; and Mason, E. A.: Properties of Gases at Very High Temperatures. Phys. Fluids, vol. 1, no. 5, Sept.-Oct. 1958, pp. 370-383.

35. Mason, E. A.; and Saxena, S. C.: Approximate Formula for the Thermal Conductivity of Gas Mixtures. *Phys. Fluids, vol. 1, no. 5, Sept-Oct. 1958, pp. 361-369.*

36. Moore, Jeffrey A.; and Pallone, Adrian: Similar Solutions to the Laminar Boundary-Layer Equations for Nonequilibrium Air. RAD TM-62-59 (Contract AF 04(694)-158), AVCO Corp., July 10, 1962.

NASA-Langley, 1972 — 12 L-8514

NATIONAL AERONAUTICS AND SPACE ADMINISTRATION
WASHINGTON, D.C. 20546

OFFICIAL BUSINESS
PENALTY FOR PRIVATE USE $300

SPECIAL FOURTH-CLASS RATE
BOOK

POSTAGE AND FEES PAID
NATIONAL AERONAUTICS AND
SPACE ADMINISTRATION
451

U.S.MAIL

POSTMASTER: If Undeliverable (Section 158 Postal Manual) Do Not Return

"The aeronautical and space activities of the United States shall be conducted so as to contribute . . . to the expansion of human knowledge of phenomena in the atmosphere and space. The Administration shall provide for the widest practicable and appropriate dissemination of information concerning its activities and the results thereof."

—NATIONAL AERONAUTICS AND SPACE ACT OF 1958

NASA SCIENTIFIC AND TECHNICAL PUBLICATIONS

TECHNICAL REPORTS: Scientific and technical information considered important, complete, and a lasting contribution to existing knowledge.

TECHNICAL NOTES: Information less broad in scope but nevertheless of importance as a contribution to existing knowledge.

TECHNICAL MEMORANDUMS: Information receiving limited distribution because of preliminary data, security classification, or other reasons. Also includes conference proceedings with either limited or unlimited distribution.

CONTRACTOR REPORTS: Scientific and technical information generated under a NASA contract or grant and considered an important contribution to existing knowledge.

TECHNICAL TRANSLATIONS: Information published in a foreign language considered to merit NASA distribution in English.

SPECIAL PUBLICATIONS: Information derived from or of value to NASA activities. Publications include final reports of major projects, monographs, data compilations, handbooks, sourcebooks, and special bibliographies.

TECHNOLOGY UTILIZATION PUBLICATIONS: Information on technology used by NASA that may be of particular interest in commercial and other non-aerospace applications. Publications include Tech Briefs, Technology Utilization Reports and Technology Surveys.

Details on the availability of these publications may be obtained from:

SCIENTIFIC AND TECHNICAL INFORMATION OFFICE

NATIONAL AERONAUTICS AND SPACE ADMINISTRATION

Washington, D.C. 20546